Continental Shelf Research
March-April 2005; 25 (5-6) : 629-653
http://dx.doi.org/10.1016/j.csr.2004.10.003

Coupling physical and biogeochemical processes in the Río de la Plata plume

Martin Huret[a, b], Isabelle Dadou[a], Franck Dumas[b], Pascal Lazure[b] and Véronique Garçon[a, *]

[a] LEGOS/CNRS, 18, Avenue Edouard Belin, 31401 Toulouse Cedex 9, France
[b] IFREMER Centre de Brest, BP 70 29280 Plouzané, France

* Corresponding author.: veronique.garcon@cnes.fr (V. Garçon), Fax: +3356 125 3205

Abstract:

A coupled three-dimensional physical-biogeochemical model was developed in order to simulate the ecological functioning of the Rio de la Plata estuary and plume. The biogeochemical model reproduces the nitrogen cycle between five compartments: dissolved inorganic nitrogen, phytoplankton, zooplankton, detritus and dissolved organic nitrogen. The coupling is tested in seasonal climatological configurations and for the particular year 1999. The circulation is forced with Parana and Uruguay rivers discharges, NCEP wind and tide. The biogeochemical model includes loads of inorganic and organic nitrogen from both rivers. The model reproduces the correct tidal amplitudes in the estuary, as well as the most outstanding features of the observed horizontal and vertical structures of the salinity plume. Simulated surface chlorophyll a concentrations exhibit maximum values all year long seaward of the turbidity front, between the 0.5 and 15 isohalines, in agreement with SeaWiFS images of the area. The model simulates well the low primary production in the light-limited highly turbid tidal river (20 gC/m(2)/yr), the high production area in the frontal zone where it can reach 500 gC/m(2)/yr, and the nutrient-limited production in the outer estuary and inner shelf (300 gC/m(2)/yr), with realistic values in each case. According to the 1999 model simulation, the tidal river is the location of organic nitrogen remineralization with a consequent increase of the inorganic pool. At the entrance of the frontal zone, inorganic nitrogen represents about 75% of the whole nitrogen pool, it is reduced to 50% at its sea end-member. The outer estuary has the same sink role for inorganic nitrogen, suggesting that organic nitrogen is the major form exported to the shelf..

1 Introduction

The Río de la Plata estuary, located along the South East coast of South America, between Argentina and Uruguay, drains the second largest basin of the South American continent. The Paraná and Uruguay rivers are the main tributaries with more than 97% (Nagy et al., 1997) of the 22 000 m^3/s long-term mean runoff (the sixth largest in the world, Shiklomanov, 1998). Both capitals Buenos Aires and Montevideo lie on either shore of the estuary. This is also a valuable system for fisheries, with its outer part being the spawning and nursery area of many fish species (Nion, 1997). The Río de la Plata system is highly sensitive to changes in nutrient loading and freshwater input, which may modify the ecosystem structure by the development of harmful algal blooms and consequent eutrophication (Nagy et al., 2002). Both Paraná and Uruguay rivers are sensitive to ENSO-induced variability in flow (Depetris and Kempe, 1990; Mechoso and Iribarren, 1992), which results from coherent ENSO-related precipitation over Southeastern South America (Ropelewski and Halpert, 1987). Over the 1983-1992 period, a noticeably increased trend in the mean river discharge, which has reached 25 000 m^3/s, has been associated to stronger ENSO events (Nagy et al., 1997).

The Río de la Plata system, as many coastal zones, is specially vulnerable to climate change. Developing adaptation and mitigation strategies to cope with such changes requires modelling as a predictive tool for the system evolution. Within the IGBP/LOICZ (Land-Ocean Interaction in the Coastal Zone) core project, two budget models have been adapted to the outer estuary (Smith, 1997) and to the frontal region of the Río de la Plata (Nagy, 2000). Such box models provide robust estimates of the variable fluxes (N and P in their case) at steady-state across boundaries, from mean *in-situ* values of these variables. However they do not allow to study the variability of these fluxes, neither to comprehensively understand the internal coupling between physical and biogeochemical processes of the system.

Here we made a step forward by developing a system model of the area, referring to the LOICZ classification (Gordon et al., 1996). Constant increases in computer power has led to the development of fully 3-D coupled physical-biological models at the shelf, coastal, and estuarine scale (see James (2002) for a review of coastal model applications and present capabilities). Such models are particularly necessary when modelling systems with strong vertical structures such as the Río de la Plata. A three dimensional modelling work of the Río de la Plata has already been implemented to study the plume dispersion in climatological situations (Simionato et al., 2001). In the present paper we coupled a biogeochemical model to an hydrodynamical model of the estuary and shelf. We used the MARS-3D circulation model developed by Lazure and Salomon (1991) to investigate coastal hydrodynamics, with an application to

the Loire and Vilaine estuaries in France. Further applications of this model have been performed, one to simulate the dynamics of river plumes in the Bay of Biscay (Lazure and Jegou, 1998), and another to investigate the forcing effects on the subtidal circulation of Patos Lagoon, Brazil (Moeller Jr. et al., 2001).

Many ecosystem models, with different levels of functional complexity have been coupled to 3-D box or fine-grid physical models over coastal areas. They often include phytoplanktonic functional groups and multiple limiting nutrients, such as the NORWECOM model with seven prognostic variables which was used to estimate the impact of the nutrient reduction in the North Sea (Skogen et al., 1995). Models of increasing complexity were used in the investigation of eutrophication process in the Bay of Seine (Guillaud et al., 2000) or in the Chesapeake Bay (Cerco and Cole, 1993). ERSEM (Baretta et al., 1995) is one of the most complete of the actual ecosystem models, with coupling to a benthic submodel ; it has been implemented for different applications in european regional seas (Allen, 1997; Paetsch and Radach, 1997; Lenhart et al., 1997; Petihakis et al., 2002). This increasing complexity has however a major drawback, which is a dramatic increase in the number of degrees of freedom combined with the lack of data for a complete validation of the different variables. For that reason and because this is one of the first attempts to model the biological activity of the Río de la Plata, we chose to keep the model structure as simple as possible, i.e. representing only the major biogeochemical pelagic variables that can be validated by available data. Consequently major biogeochemical characteristics can be evaluated for the plume, along with an estimation of nitrogen export from the estuary to the shelf, and in future work from the shelf to the open ocean. This has also the advantage to provide a fast-running model that can be tested in different configurations.

Nitrogen is generally regarded as the limiting nutrient for primary production in the oceans. In estuaries and coastal areas, N and P supplies have been considerably increased by human activity, modifying the N:P:Si ratio of seawater (Jickells, 1998). However, in most coastal areas, nitrogen seems to remain the major depleted nutrient, as it is the case for the Río de la Plata (Nagy et al., 1997). We thus adopted the simple nitrogen-based N(Dissolved inorganic Nitrogen) - P(Phytoplankton) - Z(Zooplankton) - D(Detritus) model used by Oschlies and Garçon (1999) in the North Atlantic ocean, to which we added a DON (Dissolved Organic Nitrogen) compartment. DON supply by rivers to coastal areas is significant, and the subsequent DON pool is of great contribution to biological activity in estuaries and adjacent coastal waters (Seitzinger and Sanders, 1997; Nedwell et al., 1999).

The paper is structured as follows. Section 2 provides a brief description of the environmental settings of the Río de la Plata. After describing the coupled physical and biogeochemical model in section 3, analysis results from both a

climatological simulation and a realistic year (1999) simulation are presented in sections 4 and 5. Interests of the model in providing fluxes between biogeochemical compartments in the different parts of the Río de la Plata are highlighted, together with the key role of the highly sensitive and biologically important frontal zone of the estuary in both sections 5 and 6.

2 The Río de la Plata environment

The physical oceanography and the sediment transport processes of the Río de la Plata estuary and plume are well understood and documented, through many *in-situ* studies leading to long period analysis (Guerrero et al., 1997; López Laborde and Nagy, 1999; Framiñan et al., 1999), and from remote-sensing which allows a more synoptic view of the whole estuary (Gagliardini et al., 1984; Framiñan and Brown, 1996).

This 320 km long funnel-shaped estuary can be divided in two distinct morphological areas (Fig.1) : the shallow highly turbid tidal river, and the 230 km wide outer estuary open to the shelf. They are separated by a turbidity front, closely related to the salinity one, that has been studied in details with the satellite sensor NOAA-AVHRR by Framiñan and Brown (1996). This front mean location coincides with the 5 m isobath at the southern coast and follows the Barra del Indio geometry across the river (see Fig.2). However its extent and location are highly variable depending on the river discharge and wind forcing. Suspended matter behavior in the outer estuary is quite different between the Uruguayan coast, where intense discharge flows out and disperses the matter, and the shallow tidal mixed Samborombón Bay where the matter remains trapped (López Laborde and Nagy, 1999).

Upstream of the turbidity front, within the tidal river, primary production is likely to be strongly light limited (Acha et al., 2004). The small euphotic to mixing depth ratio should not allow a positive net primary productivity (Cloern, 1987). The region of low salinity in temperate estuaries is often the location of a Maximum Turbidity Zone where active physico-chemical processes such as flocculation occur (Herman and Heip, 1999). This zone was already noticed in the Río de la Plata by Ottmann and Urien (1966). Downstream of this maximum, the concentrations of dissolved inorganic nutrients generally decrease rapidly as phytoplankton biomass increases along the salinity gradient (Malone et al., 1988; Jickells, 1998; Nedwell et al., 1999). Such a phytoplankton biomass distribution related to turbidity has been described for other major river plumes like the Mississippi (Lohrenz et al., 1990) or the Amazon (Smith Jr. and Demaster, 1996). In our estuarine system, the drawdown process of inorganic nitrogen occurs in the 3-18 salinity range (Nagy and Blanco, 1987; Blanco, 1989).

On the inner shelf, the strong salinity plume of the Río de la Plata plays a major role in the dynamics, modifying the vertical structure of water masses (Piccolo, 1998; Piola et al., 2000). The influence of the plume has even been noticed along the Brazilian coast as far as 23^{o}S (Campos et al., 1999). However, many questions remain, on its real hydrodynamical and biogeochemical impact over the shelf and finally on exported matter to the open ocean.

3 Description of the coupled three-dimensional model

3.1 The physical model

The MARS three dimensional free-surface model uses a finite difference scheme to solve the entire set of primitive equations. This allows calculation of currents, temperature, salinity and dispersion of suspended and dissolved elements. The numerical integration method is of Alternating-Direction Implicit (ADI) type (Peaceman and Rachford, 1955). The equations are solved using a split external-internal mode (Blumberg and Mellor, 1987), which means running together a 2D model for the surface elevation and barotropic currents, and a 3D model for baroclinic currents. Vertical fluxes are calculated implicitly. Vertical eddy viscosity and diffusivity are calculated by the resolution of the turbulent kinetic energy equation, with an algebraic formula for the mixing length. Turbulent horizontal diffusion coefficients are set constant and as weak as possible (20 m^2s^{-1}) just to ensure numerical stability. The adaptive time step is around 1000 s. The model is in spherical coordinates, giving an approximate horizontal resolution of 7 km at mid-latitudes. The sigma coordinates system we chose allows to work with a constant number of points in the water column, despite the heterogeneous bathymetry and the free surface ability of the model. There are 15 levels on the vertical, with thinner thicknesses for bottom and surface than for mid-layers.

The simulated domain extends from 30^{o}S to 41^{o}S, and from 48^{o}W to 63^{o}W (Fig.1), including the continental margin and a part of the Argentinean Basin with a maximum depth of 5500 m. The bathymetry has been built from *in-situ* data (Woodworth, pers. com.), combined with ETOPO5 in areas where *in-situ* data were not sufficient. This bathymetry (Fig.2) gives very realistic features in the Río de la Plata as compared with the bathymetry given by Cavallotto (1987). Main channels are present : the Northern and Intermedio Channels in the tidal river, and the Oriental and Maritime ones in the outer estuary, with the English Bank separating them. The Barra del Indio separates the tidal river from the outer estuary, and the Samborombón Bay is a shallow area in the southern part of the outer estuary.

Forcing and boundary conditions.
In a recent review on the western South Atlantic continental shelf hydrography, Piccolo (1998) showed that even if the general circulation and water masses of the region were known, the real influence of the confluence of the Brazil and Malvinas currents, of the wind, and of the Río de la Plata on the shelf circulation remains to be determined. The latter is however the main driver of the dynamics of the inner shelf offshore the northern Buenos Aires Province. Even if there is evidence of interaction in the Confluence zone, of the shelf front and the main currents with the shelf waters, we chose in this study to force the circulation only with tide, river run-off, and wind. No large scale circulation is then taken into account as boundary current conditions.

Tides.
The open boundary surface elevation conditions are produced by a larger barotropic 2D model extending from 25^{o}S to 50^{o}S and from 46^{o}W to 70^{o}W. Its resolution is about 14.5 km in latitude and 11 km in longitude. It is forced by the 8 principal tidal components from the FES99 model (Finite Element Solution) (Lefèvre et al., 2002) at its boundaries and by wind at the air-sea interface. The amplitude of M2, which explains 80% of the total spectral energy, is plotted on Fig.3a. Compared to the tidal chart of the same component (see Fig.8.2 in Framiñan et al., 1999), modeled amplitudes are slightly higher in our case in the outer estuary, whereas they are lower in the tidal river. The general southward increase in the estuary is well reproduced. Furthermore, the amplitude of 60 cm in the Samborombón Bay, where it reaches its maximum, is close to the modeled amplitude of 65 cm given by Simionato et al. (2001). The nearly complete wavelength present within the estuary at all times is also well reproduced in our model, with co-phase lines perpendicular to the estuary axis (Fig.3b). Given these low tidal amplitudes, main water level fluctuations are produced by weather patterns in the Río de la Plata. The extended 2D model is independently run to provide the nested 3D model with consistent boundary conditions.

Rivers.
Freshwater inputs to the Río de la Plata are supplied by the Paraná and Uruguay rivers. The monthly discharge data were provided by the Subsecretaria de Recursos Hidricos of Argentina (*http://www.obraspublicas.gov.ar/hidricos/*). The Túnel Station (31^{o}41'50"S, 60^{o}30'40"W) is used for the Paraná discharges, and Paso de los Libres Station (29^{o}43'S, 57^{o}04'W) for the Uruguay discharges. The latter station is located upstream of a major reservoir lake (Salto Grande), for which the residence time of water inside is a few days. It is difficult to evaluate the net biogeochemical/hydrological effect of this reservoir on the biogeochemistry of the river.

Surface fluxes.
Wind is computed from NCEP model reanalysis wind stress, interpolated on

our model grid. Rainfall, evaporation and groundwater freshwater fluxes can be ignored in this very large river-dominated system. Surface heat fluxes are not considered here. Vertical stratification generated by salinity differences can be strong, but the temperature in the Río de la Plata estuary remains almost vertically homogeneous during the winter and summer seasons (Framiñan et al., 1999). On the continental shelf, typical development and breakdown of the thermocline play an important role in setting the primary production (Carreto et al., 1995). However, as our study focuses mainly on the Río de la Plata plume, the temperature field is fixed homogeneously constant to 15^{o}C, the approximate mean annual temperature of the estuary. The temperature of the river input is set identical to the estuary temperature field.

3.2 The biogeochemical model

Coupling a biogeochemical model to a 3D hydrodynamical model means considering the evolution of a tracer concentration C_i, determined by the advective-diffusive equation of the physical model plus a source-minus-sink (sms) term of exchange between different tracers, which reads with σ coordinates :

$$\frac{\partial HC_i}{\partial t} = -\frac{\partial H(uC - \mathcal{K}x\frac{\partial C_i}{\partial x})}{\partial x} - \frac{\partial H(vC - \mathcal{K}y\frac{\partial C_i}{\partial y})}{\partial y} - \frac{\partial (wHC_i - \frac{\mathcal{K}z}{H}\frac{\partial C_i}{\partial \sigma})}{\partial \sigma} + sms(C_i) \tag{1}$$

with H the depth of the grid box. The terms on the right-hand side are the three-dimensional advection of the tracer by the velocity field, the horizontal diffusion in both directions with coefficients $\mathcal{K}x$ and $\mathcal{K}y$, the vertical mixing with turbulent diffusion coefficient $\mathcal{K}z$, and the source-minus-sink term. The formulation of the latter for each of the biological tracers of our model, with the parameter values (Table 1), is given by :

$$sms(N) = \rho DON + (1 - f_2)\gamma Z - J(z,t,N)P \tag{2}$$

$$sms(P) = (1 - \varepsilon)\ J(z,t,N)P - G(P)Z - \mu_p P \tag{3}$$

$$sms(Z) = f_1 G(P)Z - \gamma Z - \mu_z Z^2 \tag{4}$$

$$sms(D) = (1 - f_1)\ G(P)Z + \mu_p P + \mu_z Z^2 - \mu_d D - w_s \frac{\partial D}{\partial z} \tag{5}$$

$$sms(DON) = \varepsilon\ J(z,t,N)P + f_2\gamma Z + \mu_d D - \rho DON \tag{6}$$

The phytoplankton growth J uses the minimum of light and nutrient limitation, defined as

$$J(z,t,N) = \min(J(z,t), J_{\max}\frac{N}{k_N + N}) \tag{7}$$

in which $J(z,t)$ is the purely light limited growth rate, and $J_{\max} = ab^{cT}$ is the light saturated growth rate.

The light availability for photosynthesis at depth z is defined by

$$I(z,t) = PAR \times I_0(t) \exp^{-(K_w z + \int_0^z (K_c P(z) + K_{spm} SPM(z))dz)} \tag{8}$$

where PAR stands for a constant which converts incident surface irradiation I_0 to photosynthetically active radiation, and SPM is the concentration of the non-organic part of the suspended particulate matter. Then, $J(z,t)$ is calculated following Evans and Parslow (1985) :

$$J(z,t) = \frac{J_{\max} \alpha I(z,t)}{\sqrt{[J_{\max}^2 + (\alpha I(z,t))^2]}} \tag{9}$$

In the case of our climatological simulations (see Part 3.3), where we use climatological shortwave radiations, the calculation of $J(z,t)$ is done following Oschlies and Garçon [1999], meaning that J is averaged in time over one day and in the vertical over one grid box. When the diurnal cycle is included in the forcing, (see Part 3.4), J is only averaged vertically. In both cases, the integration to calculate J is solved analytically as described by Evans and Parslow (1985).

As we have no information on SPM concentrations measured in the field for our simulation period, SPM is calculated as an inverse exponential function of salinity, as plotted from *in-situ* data by Nagy and Blanco (1987). A maximum value (for the tidal river freshwater) of 150 mg/l was chosen, even if values up to 300 mg/l may be found in this part of the estuary (López Laborde and Nagy, 1999). This simulates a highly turbid area in the tidal river, with a marked turbidity front in the salinity range 0.5-5. This simple formulation gives a mean turbidity situation in agreement with what is commonly observed (Framiñan and Brown, 1996; Framiñan et al., 1999), but does not allow to reproduce local or non-linear physical phenomena leading to sediment erosion or deposition. A further step in such a modelling work would be to constrain turbidity by data on particulate matter supply to the estuary, and by coupling with a sedimentological model.

The phytoplankton capture rate is given by the following Holling type III function :

$$G(P) = \frac{gpP^2}{g + pP^2} \tag{10}$$

with g and p defined in table 1.

As deposition and resuspension of sediments are not modeled here, we state

that $w_s \frac{\partial D}{\partial z}$ is set to zero in the bottom layer. This means that all detritus are hydrolyzed and then remineralized, without organic matter lost to the sediments.

The advection-diffusion of biological tracers, as well as the sms terms, are calculated with the same time step as the physical model. The boundary conditions for tracers concentrations when the current is oriented inside of the model area is forced with the value directly inside of the realm. This approximation does not affect results since the distance of the Río de la Plata to the boundaries of the model area is large enough.

3.3 Climatological simulations

As a first step toward validation of the coupled model, we tested the effect of simple climatological forcing and configurations presented in Table 2. In addition to two typical seasonal experiments, we tested the effect of a strong discharge (40 000 m^3/s), mimicking a flood event connected to ENSO (see the high discharges of fall 1998 on Fig.4). In all three numerical experiments, we use wind, river discharge and tides. The initial salinity field is set to 35. The climatological stationary wind is computed from NCEP wind stress of the 1990-2000 period (Fig.5). Austral summer is defined as January-February, austral winter as July-August, following Simionato et al. (2001). Wind stress fields are very similar to those of Simionato et al. (2001), despite the fact we used a longer climatology (1990-2000) than they did (1991-1995). Summer is characterized by predominance of westward winds (Fig.5b). In winter, mean wind stresses are weak over the Río de la Plata (Fig.5a), even if strongest winds may occur during this season. In the outer part of the estuary, winds are northeastward, as confirmed by meteorological data (Framiñan et al., 1999). Net shortwave radiation is also from the NCEP climatology over the same period, but the mean value covering the Río de la Plata estuary is used as a typical value for the whole domain. Winter and summer mean discharge values, calculated from the mean monthly discharges, do not show a marked difference (Table 2). As explained by Nagy et al. (1997), there is no clear seasonal cycle for the Río de la Plata discharge, even if both the Paraná and the Uruguay have their own seasonal cycle. The values we use are close to the mean long trend annual average value of 22 000 m^3/s (Framiñan et al., 1999).

The first attempt was to test the hydrodynamical settings on the biological response. Consequently, biogeochemical configurations are identical for both seasons. Only few data are available on the Paraná and Uruguay rivers geochemistry. Depetris and Kempe (1993) reported for the Paraná river, between March 1981 and May 1982 (Pre-ENSO period), discharge-weighted means of 0.3 mg/l for the Particulate Organic Nitrogen (PON), and 6.1 mg/l for the

Dissolved Organic Carbon (DOC). Mañosa and Depetris (1993) reported for the Uruguay river between December 1985 and June 1986, discharge weighted means of 0.09 mg/l for PON and 3.4 mg/l for DOC. C:N ratio is not available on DOC, a mean value of 10 was considered to estimate the DON concentrations (Probst, pers. com.). Weighting by the Paraná and Uruguay rivers' discharges, we have a value of 0.25 mg/l for PON, and 0.63 mg/l for DON. Nitrate and DOC concentrations were also measured during different months over the 1993-2001 period (Probst, pers. com.). Mean values of 13.5 mmolN/m^3 for nitrate in the Paraná and 28.5 mmolN/m^3 in the Uruguay river are obtained. Mean values of DOC were 4.15 mg/l for the Paraná, and 7.8 mg/l for the Uruguay. This gives a value of 17.3 mmolN/m^3 (0.25 mg/l) for NO_3^-, and 0.58 mg/l for DON, which is really close to the DON value above. The selected values are summarized in Table 2. We assume here that nitrate is the only constituent of the dissolved inorganic nitrogen (DIN). However, another source of dissolved inorganic nitrogen for the Río de la Plata estuary is the ammonium sewage from the cities of Montevideo and Buenos Aires. Nitrogen atmospheric deposition to the ocean is also ignored here, even if it can be an important input to coastal areas (Jickells, 2002).

Initial biological field conditions are identical between the different experiments (Table 2). Open ocean and shelf tracers fields are very different, between the northern and southern parts of the realm area, with regard to the location of the confluence between the Brazil and Malvinas currents. However, as we do not model the general circulation, no difference is represented in our initial conditions, and typical values of the offshore waters of the Río de la Plata are used (Table 2). Focusing on the plume, this should have little effect, considering the predominant role of the river on the physical and biological activity in that area. Phytoplankton and zooplankton initial conditions are modeled as an inverse exponential function of depth, DIN as a linear function of depth. DON and PON were set to a small value of 10^{-4} mmolN/m^3.

3.4 One year simulation

To evaluate the seasonal variability of the biological activity in the Río de la Plata estuary and plume, we carried out an experiment where the model is integrated over a one year period. The year 1999 was particularly adapted for that, despite its characteristics due to La Niña conditions. Indeed, ecological conditions were already described by Nagy et al. (2002) for two months of this year from *in-situ* data. In addition, many cloud-free SeaWiFS (Sea-viewing Wide Field-of-view Sensor) images are available, allowing us to validate surface chlorophyll *a* concentrations from the model.

NCEP 6 hours wind stress and net shortwave radiations are used. Thus, the

light limitation growth rate is interpolated over each grid box, and is constant during the 6 hours averaged shortwave values. Daily river discharges are not available, they are thus interpolated from the mean monthly discharges. These freshwater inputs are presented on Fig.4 for the period 1998-1999. As noticed before in the climatological settings, no clear seasonal cycle stands out during this period. The "El Niño" year 1998, which is used as a one year spin-up, shows very high discharges for both rivers, with more than 40 000 m^3/s during fall. Annual cycles of DON and DIN rivers supply were built from the pluri-annual sampling from J.L. Probst (pers. com., see 3.3), for both rivers. PON concentrations are 0.3 mg/l for the Paraná (Depetris and Kempe, 1993) and 0.09 mg/l for the Uruguay (Mañosa and Depetris, 1993). Depetris and Kempe (1993) showed a strong difference between ENSO and pre-ENSO concentrations in organic particulate matter. A value of 0.13 mgN/l was measured during ENSO conditions. We therefore adjusted the PON concentration to 0.13 mgN/l for the model year 1998.

The model is run after a one year spin-up with the NCEP realistic forcing of the year 1998, and with initial physical and biological field conditions deduced from the climatological simulations.

4 Results on climatological simulations

4.1 Salinity distribution in the winter and summer regimes

Results are presented after a 5 months integration period. At this stage, the salinity front is established around the limit of the tidal river, and the ecosystem model is in a balanced state.

The two first experiments are characterized by distinct wind forcing for the physics, and distinct shortwave radiation for the biology (Table 2). Main features for surface salinity (Fig.6a,b) are similar to the results found by Simionato et al. (2001) (see Fig.4e and 4f in their paper). In winter (Fig.6a), the preponderant winds are westerlies, but with a quite low intensity over the estuary area. As suggested by Simionato et al. (2001), the northward orientation of the plume during this season is mainly explained by the Coriolis effect on the Río de la Plata discharge. The isohalines are more constrained in the interior of the estuary in its southern part as compared to Fig.4f of Simionato et al. (2001). In summer (Fig.6b), driven by preponderant easterly winds, the low salinity plume is constrained inside of the estuary in its northern part, whereas it expends southward on its southern part driven by the Ekman transport.

The surface and bottom salinity (latter not shown) distributions have been compared to data derived isohalines (Framiñan et al., 1999)(see Fig.8.7 in their paper). Even if these data gather two different seasons (fall/winter and spring/summer) which do not correspond exactly to our simulations, it is interesting to notice that data give the same southward expansion for the summer case, and a northeastward expansion for the winter case. However, our isohalines higher than 30 are inside the estuary on the north for the summer case (Fig.6a), and inside on the south for the winter case (Fig.6b). These differences with observed salinities can be attributed to the intra-seasonal variability or residual low salinity waters from a previous location of the plume, two effects obviously not included in our climatological simulations. Another possible discrepancy source is additional freshwater supply, also not considered here, particularly from Patos Lagoon, that could explain the observed southward extension of the 33 isohaline offshore the Uruguayan coast (Fig.8.7.b in Framiñan et al., 1999), as suggested by Guerrero et al. (1997).

Looking at the 5 and 10 isohalines, the model shows an offshore extension, particularly for the surface 10 in the Maritime Channel in summer, corresponding to a strong haline stratification in both seasons (see Fig.6e,f) due to the Río de la Plata discharge. In our climatological simulations, constant winds without strong episodic meteorological events participate in this stratification. In winter, the stratification occurs in the Maritime Channel as in the Oriental Channel (Fig.6c,e). An example of winter sections is given in Guerrero et al. (1997) (Fig.8 in their paper), that confirms this general stratification and depth of isohalines during this season with a further offshore extension of the estuarine waters along the northern section. In summer, the stratification occurs only in the southern outer estuary (Fig.6f), whereas isohalines are almost vertical in the Oriental Channel. The closest section in time available in Guerrero et al. (1997) for this period is from November (see their Fig.9), and their northern section also shows vertical isohalines in the Oriental Channel. The 0.5 isohaline shows a large intrusion in the northern inner part of the estuary in the summer case (Fig.6b). This reveals the preference for the flow to go through the Intermedio Channel rather than through the Northern Channel and then the Oriental Channel, in such a wind configuration enhancing the Ekman transport to the south.

4.2 Chlorophyll distribution in the winter and summer regimes

Chlorophyll *a* concentration is chosen here as a proxy of biological activity in both seasons. The chlorophyll *a* concentration is diagnosed from the phytoplankton concentration by assuming a constant C:Chl-a ratio (50 mgC per mgChl-a), and a Redfield ratio C:N of 106:16. Nitrogen supplied by both rivers into the Río de la Plata remains available in the whole estuary, and

consequently is not a limiting factor for primary production. Thus the only limitation factor is light availability. This explains the strong difference between chlorophyll *a* concentration distribution in winter and summer (Fig.7). In winter, maximum values of 3 mgChl-a/m^3 are located at the surface in the Maritime Channel (Fig.7a and c), where the surface stratification is very shallow and thus mixing depth small enough, as compared to the Oriental Channel (Fig.6c and e). In the tidal river, no production is possible due to the excessive light limiting turbidity. In summer, chlorophyll *a* concentration can reach values of 30 mgChl-a/m^3 in the low surface salinity tongue and in the Samborombón Bay (Fig.7b). Production can also occur in the Northern Channel in the tidal river. As seen before on Fig.6b, salinity is higher than 0.5 in this area, which means that turbidity is lower than in other parts of the tidal river, considering our SPM parameterization as a function of salinity ; consequently phytoplankton growth is allowed.

4.3 Experiment of a flood event

In comparison with the winter configuration described above, the flood event surface salinity is shown on Fig.8a. The effect of such a discharge would be to extend northeastward the low salinity plume, with the 5 isohaline reaching the mouth of the estuary. In a comparative work to explain the occurrence of low salinity waters as far north as 22^{o}S, Pimenta et al. (2002), using the Princeton Ocean Model, noticed that with a discharge of 50 000 m^3/s, the plume could reach a latitude of 28^{o}S after 130 days of simulation, whereas it only reached 32^{o}S with a discharge of 25 000 m^3/s. After the same time integration of our model and our winter discharge of 22 500 m^3/s, our modeled plume reaches 30^{o}S. The difference might be due to the wind forcing we use, which increases the northern deviation of the plume. In our flood experiment (40 000 m^3/s) where no wind forcing was introduced, the 33 isohaline extension goes up to the northern boundary 30^{o}S of the modeled realm, in potential agreement with the Pimenta et al. (2002) results.

Surface chlorophyll *a* concentration is high, after 5 months of this flood simulation, in the northern outer estuary and along the Uruguayan coast within the 20 isohaline (Fig.8b). Maximum values around 40 mgChl-a/m^3 can be found, although shortwave radiation forcing used is the same as in our winter experiment. To understand if this is due to the stronger nutrient supply, to the increased stratification due to higher discharge, or to the wind absence, the same simulation was performed including the winter wind. In this case (not shown), chlorophyll *a* levels are only slightly higher than those of the winter case (Fig.7a), with an offshore displacement of the features. This result suggests that under light wind conditions, bloom occurrence is possible during the light limiting season, which is confirmed on some winter SeaWiFS

images (not shown). It is also likely that strong discharge events participate in increasing primary production by strengthening the haline stratification.

5 The year 1999 simulation

5.1 Biological activity in the Río de la Plata plume

Four months were selected from our simulation to characterize the seasonal evolution of the biological activity in the Río de la Plata plume. We chose March, June, September and December because they were well representative of the different situations revealed by our model, and because we have several cloud-free SeaWiFS images from the HRPT station of Buenos Aires available for these particular months.

The realistic forcings used in this simulation increase the agreement between the modelled monthly mean salinity surface fields (Fig.9A) and some of the patterns from the long-term climatology of Framiñan et al. (1999). The extension of high values isohalines in the northern part of the shelf is more a constant feature along the year. The salinity front location delimited by the 0.5 and 5 isohalines is in accordance with its average known location, with a further offshore extension from June to September because of stronger discharges (Fig.4) and offshore winds dominance. The summer intrusion of the 0.5 isohaline in the Northern Channel disappeared as compared with the summer climatological simulation, the tidal river being all year long filled with freshwater. However, the modelled year 1999 shows also peculiarities as compared with the long term trend, one of them being a preference for the plume to extend in the southern direction during the winter season (June to September) rather than during the summer one (December to March).

5.1.1 Modelled seasonal patterns of chlorophyll a

Surface chlorophyll *a* concentrations from the model are presented on Fig.9B. In March, the concentration is high in the frontal zone until the 20 isohaline with values reaching 30 mgChl-a/m^3. The concentration is also quite high over the influenced shelf with values often higher than 2 mgChl-a/m^3 in the plume oriented to the north. In June, the chlorophyll *a* concentration is far lower in the Río de la Plata estuary, except for the shallow Samborombón Bay which shows maximum values. The plume is almost non-visible, with values lower than 2 mgChl-a/m^3 in the center of the outer estuary. In September, the outer estuary and the area limited by the 25 isohaline extension contain values close to 10 mgChl-a/m^3, which extend quite far to the north along

the Uruguayan coast. The maximum values are still located in the north of the Samborombón Bay. The December situation is quite similar to the March one. However, maximum concentrations are found upstream in the tidal river, and some high concentrations are modelled in the Northern Channel of the tidal river. Values around 3 mgChl-a/m^3 still extend to the north along the Uruguayan coast. The maximum chlorophyll levels simulated by our model are all year long located in the proximity of the turbidity front, between the 0.5 and 15 isohalines.

5.1.2 Use of SeaWiFS images over the Río de la Plata

Quantitative estimates of the surface chlorophyll *a* concentration are available daily in the case of clear sky from satellite 'ocean color' data. Since its launch in September 1997, SeaWiFS has been providing useful data for monitoring the phytoplankton biomass in Case 1 waters, i.e. waters dominated by phytoplankton and its degradation products. In coastal Case 2 waters, where suspended terrestrial matter and Color Dissolved Organic Material (CDOM) strongly influence optical properties, chlorophyll *a* concentrations estimated by classical algorithms such as Ocean Color 4 (OC4) or 2 (OC2) (O'Reilly et al., 1998) are often over-estimated, as this has been observed for the Rio de la Plata waters (Armstrong et al., 2004). A "look-up" table based upon an empirical parameterization of the OC4 ratio as a function of $L_{nw}(412)$ (Normalized Water Leaving Radiance at 412 nm) and $L_{nw}(555)$ is used by Gohin et al. (2002) to retrieve chlorophyll *a* concentration in Case 2 waters of the Bay of Biscay and the English Channel (France). The use of the $L_{nw}(555)$ is done to reduce the effect of the suspended matter load in the estimated chlorophyll *a*.

For the Río de la Plata, we do not have a set of *in-situ* data simultaneous with SeaWiFS clear images that would allow us to build a similar "look-up" table. We expect however the OC5 algorithm from Gohin et al. (2002) to provide better results than OC4 in the typical Case 2 waters of the tidal river and the frontal zone where a turbidity maximum is observed. Fig.10a,b show the possible discrepancy between both algorithms, on November 12^{th} 1999 as an example. Flags such as "turbidity", which are advised to be used with OC4 are here withdrawn, which allows us to use SeaWiFS data in the Río de la Plata, although increasing the error on estimated chlorophyll *a*. Despite this issue, very few data are available on the tidal river because of negative water leaving radiances in the low wavelengths until the 510 nm channel. As expected, OC4 gives high values (more than 25 mgChl-a/m^3) in the frontal zone, with no decreasing gradient upstream in the tidal river. Valid SeaWiFS pixels of the tidal river (on November 21^{st}, not shown) show also values higher than 25 mgChl-a/m^3. High values are also found along the coast of the Samborombón Bay with OC4, a shallow area where particulate matter resuspension often

occurs making it a turbid zone. With the OC5 algorithm, a clear decreasing gradient is visible (Fig.10a), with values of 1 mgChla/m^3 in the tidal river (same values are found in the whole tidal river on the 21^{st}). Highest values found by OC5 are located seaward of the tidal river. For this November 1999 period, Nagy et al. (2002) reported an upward displacement of the frontal zone along the Uruguayan coast, which can be seen on the OC5 image (Fig.10a) with high values of chlorophyll *a* more upstream than usual. No in-situ data allow us for now to decide whether OC4 or OC5 gives in general the most reasonable values in the clearer waters of the outer estuary and shelf.

5.1.3 Comparison of the modelled chlorophyll a with SeaWiFS images and sparse in-situ data

The discrepancy detailed above between both algorithms reveals the uncertainty we have on estimates of SeaWiFS chlorophyll *a* concentrations over typical Case 2 waters. It makes the model validation using 'ocean color' data still quite approximate. For that reason, we chose to give more importance for comparison to the seasonal cycle of the chlorophyll *a* distribution rather than to its absolute values (Fig.9C). In March, the chlorophyll *a* plume seen by SeaWiFS (OC5 algorithm) extends to the south along the Argentinean shore. This feature is not reproduced by the simulated chlorophyll *a* distribution, not even by the simulated surface salinity plume, which may explain this discrepancy. The maximum values simulated in the frontal zone are greater than those given by OC5. In June, the model produces a plume of high chlorophyll *a* values in the Maritime Channel but concentrations remain much lower than those given by SeaWiFS in the outer estuary (3 and 8 mg/m^3). The simulated very high values in the northern Samborombón Bay are not measured by the sensor. In September, values of the model are in accordance with SeaWiFS values, with an increasing gradient from the tidal river to the outer estuary. The northward extension of the plume is better reproduced than the southward one. Excessive values are still present in our model output in the northern Samborombón Bay. In December, simulated values are in the same range as OC5 over the area, except in the frontal zone and in the Northern Channel where excessive values are modelled.

Nagy et al. (2002) reported maximum values in November 1999 along the Uruguayan coast of the estuary of 28 mgChl-a/m^3, 38 mgChl-a/m^3 and 22 mgChl-a/m^3 for locations in the tidal river, in the frontal zone, and in the Oriental Channel, respectively. Our simulated values for November 12^{th} (Fig.10c) agree quite well with these measured values, and this is also the case for the monthly mean output model situation (not shown). Furthermore, the chlorophyll gradient deduced from these *in-situ* data with a maximum in the frontal zone is well simulated with our model.

5.1.4 A highly productive frontal zone

The modelled primary production integrated over the water column is given for the same months as the chlorophyll *a* (Fig.9D). In the estuary, the highest productive areas coincide with the areas with high chlorophyll *a* concentration. Primary production is very low in the tidal river; it is the highest in the front, where values of 80 gC/m^2/month can be found in March and December. If we remember the fact that the front is a shallow area with waters no deeper than 10 m, the front does represent a very productive area as compared with the adjacent marine waters of the outer estuary and even to the plume influenced shelf. At the end of autumn (June), primary productivity is very low over the estuary and shelf, whereas at the beginning of spring (September) primary productivity in the outer estuary is the same or even higher than over the shelf, with values of 45 gC/m^2/month. The high values observed offshore along the shelf slope are the result of an excessive mixing within the model in this steep area. Strong bathymetry gradient and physical processes associated to shelf slopes are still difficult to assess in hydrodynamical models. The high productivity might be artificial in our model, however it is a real feature of the shelf-break front between subantarctic shelf waters and the Malvinas current waters (Carreto et al., 1995). A variety of physical processes, still not well understood, could lead to enhance supply of nutrient-rich Malvinas current waters into the euphotic zone of this front, among them small-scale eddies or internal waves (Acha et al., 2004). Because this area is not the focus of this work, and the associated processes would need further investigation, model results in the shelf-break zone should be considered with great caution. The frontal zone shows an annual primary productivity higher than 400 gC/m^2/yr, a value reached for depth greater than 50 m over the shelf (Fig.11).

Very few measurements of primary production exist in the Río de la Plata. Smith (1997) estimated a range of 200-300 gC/m^2/yr for the outer estuary, which is the range we modelled for the outer estuary waters, seaward of the front (Fig.11). Gómez-Erache et al. (2001) gave values for January and November 1999 for the area along the Uruguayan coast of the estuary ; in their frontal zone defined by salinities lower than 5, the net primary productivity ranges from 4 to 14 gC/m^2/month during both months, and from 10 to 100 gC/m^2/month in the outer zone. The simulated November productivity fits within this range, especially in the Oriental Channel (Fig. 10d).

5.2 Biogeochemical fluxes in the frontal zone

The frontal zone between the tidal river and the outer estuary, where strong salinity and turbidity gradients occur, is a major area for biological activity. Indeed, this is the place where primary productivity can become large and

phytoplankton blooms take place. For this reason, we focussed our interest on this area, looking further in details the functioning of our biogeochemical model.

5.2.1 Nutrient evolution in the estuary

First, concentrations of different biological variables were plotted along a cross frontal zone transect (AB on Fig.11), to follow their evolution through the frontal zone up to the marine waters near 55.5^oW in the central axis of the Río (Fig.12). The zooplankton concentration evolution was not plotted as it remains very low (around 2 mmolN/m^3) as compared with other tracers.

For the first three months, evolution looks similar within the tidal river. Concentrations in DON and to a lesser extent in detritus (PON) diminish, DIN concentration increases, reflecting the input function at the Río de la Plata entrance (Fig.12f). In December, the DIN concentration remains almost constant, as phytoplankton production occurs in the tidal river (see December on Fig.9B).

In the frontal zone, the situations are very different between March and December on one hand, and June and September on the other hand. In the former case, rapid phytoplankton growth depletes the DIN concentration to levels lower than 1 mmolN/m^3. In the same time, DON and detritus increase in parallel, with the PON concentration remaining half the DON one. The dilution of tracer rich freshwaters with marine waters explains the fact that the increase in DON and PON concentrations does not compensate the decrease in DIN. In June and September, the DIN decrease is much slower and the near equilibrium final concentration is 8 mmolN/m^3 in the outer estuary, remaining higher than the concentrations of other tracers. In September, the phytoplankton concentration remains under 10 mmolN/m^3 and the increase starts late as compared with March and December. However, it lasts longer (Fig.12c) with DIN remaining available in the outer estuary, which allows a greater extension of the bloom (Fig.9B). During June, production is very low, phytoplankton concentration remains around 1 mmolN/m^3. The decrease in DIN is only due to dilution.

The evolution for the whole year 1999 (Fig.12e) shows an average situation of the seasons described above, with DIN concentration decrease starting at the entrance of the frontal zone, and the maximum phytoplankton concentration modelled at its sea end-member.

Fig.13 shows the limitation factors for surface primary production along the same axis for September (Fig.13a) and December (Fig.13b). In the tidal river, production is always light limited. In December, limitation switches in the frontal zone from light to nutrients, whereas in September, even if high phy-

toplankton concentrations can be found, nutrients never become the limiting factor in the estuary.

5.2.2 Biogeochemical fluxes between compartments

We focus now on the distribution of the different tracers within the frontal zone. We calculate fluxes between the different variables to understand the underlying biogeochemical processes setting the time variability of the simulated distributions. The budgeted area (Fig.11), with a volume of 70×10^9 m^3, is a bit larger than that used by Nagy (2000) (50×10^9 m^3).

First, Fig.14 shows the time evolution of the different variables quantity in the budget box during 1999. A clear seasonal pattern can be seen, with a DIN load more than four times greater in winter than in summer. DIN never reaches zero levels even during the summer decrease. Other tracers except zooplankton are highly correlated one to the other, and anti-correlated with DIN until spring. From October to the end of December, phytoplankton concentration remains constant whereas detritus and DON levels continue to increase. This suggests that the phytoplankton stock is at its maximum in spring, with remineralization processes limiting a greater primary production. Comparing beginning of January 1999 and 2000, quantities are similar except for the organic matter (dissolved and particulate). This difference might be due to the increase in PON supply to the estuary between the two years (see Fig.12f).

Second, cumulated fluxes between the biogeochemical compartments are calculated in the budget box during 1999 (Fig.15). The budget for each of the tracers confirms that we are close to steady-state except for the detritus and DON pools. The main nitrogen pathway follows primary production, grazing, death of zooplankton, hydrolysis of detritus and finally remineralization from DON to DIN. Input of DIN by zooplankton excretion accounts less than 15% of the total DIN input, showing the key role DON plays in our ecosystem model in this part of the estuary. Nitrogen used for primary production (32×10^9 molN) and the influx by the tidal river to the frontal zone are almost identical. This may suggest that over a year, the DIN supply to the frontal zone is potentially used for primary production, and that the nitrogen supply to the outer estuary and shelf may come from remineralization. Actually this is not really the case as there are months during which DIN is exported to the outer estuary (Fig.12b,c), meaning that part of the primary production in the frontal zone is due to DON remineralization at this location. 60% of the phytoplankton disappearance is due to grazing.

6 Discussion

6.1 Biomass and primary production

For the Río de la Plata plume, one would expect biomass pattern variations such as those found in other temperate estuaries and coastal areas. The typical case being a winter light limiting season, followed by productive spring and summer seasons, depending on the availability of nutrients. A first particularity of the Río de la Plata is its lack of a distinct seasonal discharge cycle, with alternate peaks in the runoff between the Paraná and the Uruguay rivers. The absence of a long-term nutrient monitoring for these two rivers prevents us from concluding on an annual cycle for the inorganic and organic nitrogen loads. The few data available to us, to which we may add all the urban sewages loads, together with the strong freshwater inflow, indicate that waters of the Río de la Plata plume never become nitrogen limited. The only limiting factor for phytoplankton growth would then be light. In the tidal river, this limitation occurs all year long, despite a weak production in summer. As mentionned before, it is extremely difficult to validate model outputs with satellite data. Seaward of the front, our model gives a primary production strongly reduced in winter as compared with summer (for the climatological and 1999 simulations), in agreement with the behaviour of many temperate estuaries. However, SeaWiFS monthly composites of winter months show typical bloom concentrations of chlorophyll *a* in the outer estuary (Fig.9C in June). The monthly composite is likely to overestimate the field truth mean monthly concentrations. Indeed, only very few images are available during this season, and they map bloom favorable situations because of the clear sky during these days. No *in-situ* data are available to confirm the quantitative importance of the winter biomass in the frontal zone and outer estuary.

The rough model of SPM we use does not consider the highly variable SPM concentration that can be found in the Río de la Plata estuary (see different concentrations measured since 1966 in López Laborde and Nagy (1999)). The model neither takes into account local phenomena such as dynamics of the maximum turbidity zone, or successive deposition and resuspension in shallow coastal areas. This explains the high biomass values we found all year long in the coast of the Samborombón Bay. The hydrodynamics of our model brings enough nutrients to this calm shallow area where they accumulate, but does not bring the associated SPM delivered or resuspended in the same time, that would limit the phytoplankton production along the coast.

On the shelf, seasonal biomass evolution is also poorly understood. The coastal part of the shelf is influenced by the Río de la Plata, but the main drivers of the water masses characteristics are the Brazil and Malvinas currents. They

strongly influence the northern shelf with Tropical Waters, and the southern one with Subantarctic nutrients rich Waters, respectively. The Confluence of these two currents, moving north (in winter) and south (in summer), is continued over the shelf (Piola et al., 2000), at a latitude closed to that of the estuary. In this context, it is difficult to associate the high biomass found on the shelf to the Río de la Plata or to the Malvinas influenced waters. According to measurements in front of Mar del Plata from Carreto et al. (1995), advection of Río de la Plata waters is likely to occur during spring over the southern shelf. In these instances, mixing of silicate-rich estuarine waters with nitrate rich Subantarctic waters, induces an enhanced primary production (Méndez et al., 1997). Thus, the large scale forcing with appropriate nutrients values associated to the currents seems to be a key issue to better model the shelf primary production.

For the very coastal values of the shelf, our model simulates the highest concentrations along the Uruguayan coast to the north, from spring to summer (Fig.9B see September and December) with typical values of 3 mgCh-a/m^3. These values fit within the range given by SeaWiFS imagery. Hubold (1980a) reported maximum values of 22.4 mgChl-a/m^3 near the Uruguayan coast between August and November 1977, whereas values higher than 2 mgChl-a/m^3 were present on the coastal shelf south of the estuary (our modeled values are between 1 and 2 mgChl-a/m^3 in that area). From its autumn cruise (April-June 1978), Hubold (1980b) associated the lower values found to a greater extent of the poor Tropical Waters over the shelf in the studied area. Values around 2 mgChl-a/m^3 were found at the mouth of the estuary, with a maximum value of 9.5 mgChl-a/m^3 along the Uruguayan coast. We also find lower values during autumn, which we attributed to the lower levels of irradiance since no large-scale forcing is present in our model (Fig.9B see June).

6.2 Nutrients dynamics

From Nagy et al. (2002), typical values of DIN in the tidal river between 1981-1987 are between 25 and 40 mmolN/m^3 for an average input of 23×10^9 molN/yr, with cities sewage representing 25% of the load. Nagy et al. (2002) estimated the typical freshwater end-member for DIN to be 29 mmolN/m^3. From our 1999 experiment, mean concentration in the tidal river is 50 mmolN/m^3 (see Fig.12e), with an increase toward the front. This discrepancy might be due to two main reasons. First, as suggested by Smith (1997), denitrification is likely to occur in the tidal river, leading to a DIN sink in that area and reducing the DIN supply to the frontal zone. This biogeochemical process is not considered in the model. Second, DON remineralization kinetics might be too fast in the model ; only one class of DON is included, although less labile and even refractory DON may also be found. Loss of PON to the sediment

which would reduce the PON pool to be hydrolysed into DON is also a process not considered here. To better constrain the nutrient supply to the shelf in the model, more frequent information on the different nutrient forms along the estuary would be necessary. It would finally allow us to better understand the effect of their variability on biogeochemical processes.

On the outer estuary, Nagy et al. (2002) reported values of nitrates concentration ranging between 2 and 10 mmolN/m^3, whereas values of ammonium become greater than nitrates at salinities higher than 15. Our simulation gives an average value of 5 mmolN/m^3 for DIN, with lower values between December and March (see Fig.12a,d). These are reasonable values for the outer estuary, meaning that the modelled removal of DIN in the frontal zone is strongly overestimated as compared with the long-term average of 60% found by Nagy et al. (2002). We then expect the phytoplankton biomass of the frontal zone to be greater in our simulation as compared with reality. That is actually the case in some instances when comparing our modeled chlorophyll *a* output with SeaWiFS images (Fig.9B,C).

6.3 Nitrogen export to the ocean

The export of nitrogen to the outer estuary and shelf depends on the season. As can be seen with tracer concentrations at the sea end-member of the frontal zone (Fig.12), export is essentially under an organic form (DON and PON) during summer months, whereas it is mainly inorganic during winter. Quantitatively, Fig.15 reveals that for the whole 1999 year, the first form of nitrogen export to the outer estuary is DIN (20 150$\times 10^6$ mol), despite the high primary production taking place in the frontal zone. The loss of DIN compared with what entered (32 600$\times 10^6$ mol), is mainly exported under the phytoplankton (4 435$\times 10^6$ mol) and Detritus (3 875$\times 10^6$ mol) surplus. The second form of nitrogen exported is DON (8 590 $\times 10^6$ mol). Looking at Fig.12e, DIN concentration becomes lower than DON concentration eastward of 56^{o}W, which is the shelf boundary of the estuary. This suggests that nitrogen export to the shelf is mainly under organic form. This is all the more likely, indeed production and so DIN assimilation is not the higher along the axis of the estuary, but rather in the Oriental Channel and in the south of the Maritime Channel. In this context and during highly estuarine productive months, the shelf primary production is highly dependent on remineralization. As noticed before, the absence of large-scale forcing does not allow us to extrapolate on the export from the shelf to the deep-ocean.

7 Conclusions

In order to better understand the main biogeochemical processes occurring in the Río de la Plata estuary and plume, we developed a three dimensional coupled physical-biogeochemical model. Our model realm extends on the whole shelf, but since we do not introduce the large-scale forcing (Brazil and Malvinas currents), our interpretation of the results is limited to the estuary and inner shelf. Experiments with climatological forcing, and a simulation of the year 1999, reveal a rather good agreement in the location of the salinity front and consequently of the turbidity one, given the simple relationship we used between salinity and suspended matter. This allows us to well model the effect of light limitation all year long in the tidal river, and the high primary production just seaward of the turbidity front. The exact location of the plume at the mouth of the estuary and on the shelf is not always simulated, particularly when the plume seen by SeaWiFS sensor is oriented to the south along the Argentinean coast. Introducing the large-scale oceanic influence and higher resolution on the winds pattern over the estuary and shelf might palliate this discrepancy.

The detailed study on nitrogen fluxes throughout the estuary and through the different compartments of our model, allows us to point out the major features of the system. These concern the strongly light limited tidal river, the highly productive frontal zone, and the nutrient limited outer estuary and inner shelf. It also suggests that different processes like denitrification or exchange of organic matter with the sediment would be crucial to consider in future work.

A coupled physical-biogeochemical model is a useful tool to understand processes in an estuarine system, to calculate fluxes in a budget area, or to evaluate the impact of increasing discharge (on a long-term trend or during a strong event connected to ENSO for instance). Defining eutrophication risks, monitoring of their symptoms on higher trophic levels as it is planned in the emerging IGBP/IMBER core project, are other potential applications for the Río de la Plata system.

Acknowledgements

This study was funded part by CNES and IFREMER with a fellowship support to M. Huret, and by the ACI "Observation de la Terre". The authors would like to thank the SeaWiFS Project and the Distributed Active Archive Center at the Goddard Space Flight Center, Greenbelt, MD 20771, for the production and distribution of the SeaWiFS data acquired at the Buenos Aires station. We are indebted also to NASA for providing the SeaDAS software. We are particularly grateful to F. Gohin for providing us with the OC5

look-up table and for useful discussions. NCEP reanalysis were provided by the NOAA-CIRES Climate Diagnostics Center, Boulder, Colorado, USA, at *http://www.cdc.noaa.gov/*. We also thank F. Lyard for helping us building the bathymetry, J.L. Probst and P. Depetris for providing some of the rivers biogeochemical data and constructive comments, G. Nagy for pointing out key references, A. Ménesguen, G.M.E. Perillo and an anonymous reviewer for critical reading of this manuscript.

References

Acha, E. M., Mianzan, H. W., Guerrero, R. A., Favero, M., Bava, J., 2004. Marine fronts at the continental shelves of austral South America - physical and ecological processes. J. Mar. Syst. 44, 83–105.

Allen, J. I., 1997. A modelling study of ecosystem dynamics and nutrient cycling in the Humber plume, UK. J. Sea Res. 38, 333–359.

Armstrong, R. A., Gilbes, F., Guerrero, R., Lasta, C., Benavidez, H., Mianzan, H., 2004. Validation of SeaWiFS-derived chlorophyll for the Río de la Plata estuary and adjacent waters. Int. J. Remote Sens. 25 (7-8), 1–5.

Baretta, J. W., Ebenhöh, W., Ruardij, P., 1995. The European Regional Seas Ecosystem Model, a complex marine ecosystem model. Neth. J. Sea Res. 33 (3-4), 233–246.

Blanco, A. C., 1989. Balance de masa de los silicatos en la superficie del Río de la Plata y su area de influencia en el mar epicontinental uruguayo. Thesis Lic., Fac. H. y Ciencias, Montevideo.

Blumberg, A. F., Mellor, G. L., 1987. A description of three dimensional coastal ocean circulation model. In: Heaps, N. (Ed.), Three Dimensional Ocean Models. AGU, p. 208.

Campos, J. D., Lentini, C. A., Miller, J. L., Piola, A. R., 1999. Interannual variability of the Sea Surface Temperature in the South Brazilian Bight. Geophys. Res. Let. 26 (14), 2061–2064.

Carreto, J. I., Lutz, V. A., Carignan, M. O., Colleoni, A. D. C., Marcos, S. G. D., 1995. Hydrography and chlorophyll a in a transect from the coast to the shelf-break in the Argentinian Sea. Cont. Shelf Res. 15 (2/3), 315–336.

Cavallotto, J. L., 1987. Dispersión, transporte, erosión y acumulación de sedimentos en el Río de la Plata. Informe final de beca de iniciación Comisión de Investigaciones Cientificas.

Cerco, C., Cole, T., 1993. Three-dimensional eutrophication model of Chesapeake Bay. J. Environ. Eng. 119 (6), 1006–1025.

Cloern, J. E., 1987. Turbidity as a control on phytoplankton biomass and productivity in estuaries. Cont. Shelf Res. 7 (11/12), 1367–1381.

Depetris, P. J., Kempe, S., 1990. The impact of the El Niño 1982 event on the Paraná River, its discharge and carbon transport. Palaeogeography, Palaeoclimatology, Palaeoecology (Global and Planetary Change Section) 89, 239–244.

Depetris, P. J., Kempe, S., 1993. Carbon dynamics and sources in the Paraná river. Limnol. Oceanogr. 38 (2), 382–395.

Evans, G., Parslow, J., 1985. A model of annual plankton cycles. Biol. Oceanogr. 3, 328–347.

Fasham, M., Ducklow, H., McKelvie, S., 1990. A nitrogen-based model of plankton dynamics in the oceanic mixed layer. J. Mar. Res. 48, 591–639.

Framiñan, M. B., Brown, O. B., 1996. Study of the Río de la Plata turbidity front, part 1 : spatial and temporal distribution. Cont. Shelf Res. 16 (10), 1259–1282.

Framiñan, M. B., Etala, M. P., Acha, E. M., Guerrero, R. A., Lasta, C. A., Brown, O. B., 1999. Physical characteristics and processes of the Río de la Plata estuary. In: Perillo, G. M. E., Piccolo, M. C., Pino Quivira, M. (Eds.), Estuaries of South America. Vol. 1. Springer, Ch. 8, pp. 161–192.

Gagliardini, D., Karzenbaum, H., Legeckis, R., Klemas, V., 1984. Application of Landsat MSS, NOAA/TIROS AVHRR, and Nimbus CZCS to study the la Plata river and its interaction with the ocean. Remote Sensing Environ. 15, 21–36.

Gohin, F., Druon, J. N., Lampert, L., 2002. A five channel chlorophyll concentration algorithm applied to SeaWiFS data processed by SeaDAS in coastal waters. Int. J. Remote Sens. 23 (8), 1639–1661.

Gómez-Erache, M., Nuñez, K., Lagomarsino, J. J., Nagy, G. J., 2001. Spatial heterogeneity of algal biomass and primary production in the Río de la Plata estuarine system. I Congreso Internacional Ciencia y Technología Marina, Poster Session.

Gordon, D. C., Boudreau, P. R., Mann, K. H., Ong, J. E., Silvert, W. L., Smith, S. V., Wattayakorn, G., Wulff, F., Yanagi, T., 1996. LOICZ Biogeochemical Modelling Guidelines. LOICZ Reports & Studies 5, Land-Ocean Interactions in the Coastal Zone (LOICZ), The Netherlands.

Guerrero, R. A., Acha, E. M., Framiñan, M. B., Lasta, C. A., 1997. Physical oceanography of the Río de la Plata estuary, Argentina. Cont. Shelf Res. 17 (7), 727–742.

Guillaud, J.-F., Andrieux, F., Ménesguen, A., 2000. Biogeochemical modelling in the Bay of Seine (France) : an improvement by introducing phosphorus in nutrient cycles. J. Mar. Syst. 25, 369–386.

Herman, P. M. J., Heip, C. H. R., 1999. Biogeochemistry of the MAximum TURbidity Zone of Estuaries (MATURE): some conclusions. J. Mar. Syst. 22, 89–104.

Hubold, G., 1980a. Hydrography and plankton off southern Brazil and Rio de la Plata, August - November 1977. Atlantica 4, 1–22.

Hubold, G., 1980b. Second report on hydrography and plankton off southern Brazil and Rio de la Plata ; Autumn cruise : April - June 1978. Atlantica 4, 23–42.

James, I. D., 2002. Modelling pollution dispersion, the ecosystem and water quality in coastal waters : a review. Environm. Model. and Soft. 17, 363–385.

Jickells, T. D., 1998. Nutrient biogeochemistry of the coastal zone. Science 281, 217–222.

Jickells, T. D., 2002. Emissions from the oceans to the atmosphere, deposition from the atmosphere to the oceans and the interactions between them. In: Steffen, W., Jager, J., Carson, D. J., Bradshaw, C. (Eds.), Challenges of a Changing Earth, Springer Verlag Edition. The IGBP Series. pp. 93–96.

Lazure, P., Jegou, A.-M., 1998. 3D modelling of seasonal evolution of Loire and Gironde plumes on Biscay continental shelf. Oceanol. Acta 21 (2), 165–177.

Lazure, P., Salomon, J. P., 1991. Coupled 2D and 3D modelling of coastal hydrodynamics. Oceanol. Acta 14 (2), 173–180.

Lefèvre, F., Lyard, F. H., Le Provost, C., Schrama, E. J. O., 2002. FES99 : A global tide finite element solution assimilating tide gauge and altimetric information. J. Atmos. Ocean. Technol. 19, 1345–1356.

Lenhart, H. J., Radach, G., Ruardij, P., 1997. The effects of river input on the ecosystem dynamics in the continental coastal zone of the North Sea using ERSEM. J. Sea Res. 38 (3-4), 249–274.

Lohrenz, S. E., Dagg, M. J., Whitledge, T. E., 1990. Enhanced primary production at the plume/oceanic interface of the Mississipi River. Cont. Shelf. Res. 10 (7), 639–664.

López Laborde, J., Nagy, G. J., 1999. Hydrography and sediments transport characteristics of the Río de la Plata : a review. In: Perillo, G. M. E., Piccolo, M. C., Pino Quivira, M. (Eds.), Estuaries of South America. Springer, Ch. 7, pp. 133–159.

Malone, T. C., Crocker, L. H., Pike, S. E., Wendler, B. W., 1988. Influences of river flow on the dynamics of phytoplankton production in a partially stratified estuary. Mar. Ecol. Prog. Series 48, 235–249.

Mañosa, W., Depetris, P. J., 1993. Preliminary results on carbon fluxes in the Uruguay River. In: Kempe, S., Eisma, D., Degens, E. (Eds.), Transport of Carbon and Nutrients in Lakes and Estuaries. Part. 6. SCOPE/UNEP Sonderband 74, pp. 13–22.

Mechoso, C. R., Iribarren, G. P., 1992. Streamflow in southeastern South America and the southern oscillation. J. Climate 5, 1535–1539.

Méndez, S., Gómez, M., Ferrari, G., 1997. Planktonic studies of the Río de la Plata and its oceanic front. In: Wells, P., Daborn, G. (Eds.), The Río de la Plata. An environmental overview. An EcoPlata Project Background Report. Dahlousie Univ, Halifax, Nova Scotia, Ch. 2, p. 256.

Moeller Jr., O. O., Castaing, P., Salomon, J.-C., Lazure, P., 2001. The influence of local and non-local forcing effects on the subtidal circulation of Patos Lagoon. Estuaries 24 (2), 297–311.

Nagy, G. J., 2000. Dissolved inorganic NP budget for the frontal zone of the Río de la Plata system. In: Dupra, V., Smith, S. V., Marshall Crossland, J. I., Crossland, C. J. (Eds.), Estuarine systems of the South American Region: C,N,P fluxes. LOICZ Reports & Studies 15. Texel, The Netherlands, pp. 40–43.

Nagy, G. J., Blanco, A. C., 1987. Balance de silicatos disueltos del Río de la Plata. In: 2do. Congr. Latinoam. de Ciencas del Mar. Res. p. 132.

Nagy, G. J., Gómez-Erache, M., López, C. H., Perdomo, A. C., 2002. Distribution patterns of nutrients and symptoms of eutrophication in the Río de la Plata River estuary system. Hydrobiologia 475/476, 125–139.

Nagy, G. J., Martinez, C. M., Caffera, M. R., Pedrosa, G., Forbes, E. A., Perdomo, A. C., López laborde, J., 1997. The hydrological and climatic setting of the Río de la Plata. In: Wells, P., Daborn, G. (Eds.), The Río de la Plata. An environmental overview. An EcoPlata Project Background Report. Dahlousie Univ, Halifax, Nova Scotia, Ch. 2, p. 256.

Nedwell, D. B., Jickells, T. D., Trimmer, M., Sanders, R., 1999. Nutrients in

estuaries. Adv. Ecol. Res. 29, 43–92.
Nion, H., 1997. Fishes of the Río de la Plata and some aspects of their ecology. In: Wells, P., Daborn, G. (Eds.), The Río de la Plata. An environmental overview. An EcoPlata Project Background Report. Dahlousie Univ, Halifax, Nova Scotia, Ch. 6, p. 256.
O'Reilly, J. E., Maritorena, S., Mitchell, B. G., Siegel, D. A., Carder, K. L., Garver, S. A., Kahru, M., McClain, C., 1998. Ocean color chlorophyll algorithms for SeaWiFS. J. Geophys. Res. 103 (C11), 24,937–24,953.
Oschlies, A., Garçon, V., 1999. An eddy-permitting coupled physical-biological model of the North Atlantic 1. Sensitivity to advection numerics and mixed layer physics. Global Biogeochem. Cycles 13 (1), 135–160.
Ottmann, F., Urien, C. M., 1966. Sur quelques problèmes sédimentologiques dans le Río de la Plata. Rev. Geogr. Phys. et Geol. Dyn. 17, 209–224.
Paetsch, J., Radach, G., 1997. Long-term simulation of the eutrophication of the North Sea: Temporal development of nutrients, chlorophyll and primary production in comparison to observations. J. Sea Res. 38 (3-4), 275–310.
Peaceman, D. W., Rachford, H. H., 1955. The numerical solution of parabolic and elliptic differential equations. J. Soc. Ind. Applied Math. 3 (1), 28–41.
Petihakis, G., Triantafyllou, G., Allen, J. I., Hoteit, I., Dounas, C., 2002. Modelling the spatial and temporal variability of the Cretan Sea ecosystem. J. Mar. Syst. 36 (3-4), 173–196.
Piccolo, M. C., 1998. Oceanography of the western South Atlantic continental shelf from 33^o to 55^oS. In: Robinson, A. R., Brink, K. H. (Eds.), The Sea. The global Ocean Studies. Regional studies and syntheses. Vol. 11. John Wiley & Sons, New York, USA, Ch. 9, pp. 253–270.
Pimenta, F. M., Campos, E. J. D., Miller, J. L., Piola, A. R., Camargo, R., 2002. The role of wind and river discharge on the northward extension of the Río de Plata plume, Oral Presentation. IAPSO Meeting.
Piola, A. R., Campos, E. J. D., Moeller Jr., O. O., Charo, M., Martinez, C., 2000. Subtropical Shelf Front off eastern South America. J. Geophys. Res. 105 (C3), 6565–6578.
Ropelewski, C. F., Halpert, M. S., 1987. Global and regional scale precipitation patterns associated with the El Niño / Southern Oscillation. Month. Weath. Rew. 115, 1606–1626.
Seitzinger, S. P., Sanders, R. W., 1997. Contribution of dissolved organic nitrogen from rivers to estuarine eutrophication. Mar. Ecol. Prog. Ser. 159, 1–12.
Shiklomanov, I. A., 1998. A summary of the Monograph World Water Resources. A new appraisal and assessment for the 21st Century. UNEP, Society and Cultural Organization.
Simionato, C., Nuñez, M. N., Engel, M., 2001. The Salinity Front of the Rio de la Plata - a numerical case study for winter and summer conditions. Geophys. Res. Let. 28 (13), 2641–2644.
Skogen, M. D., Svendsen, E., Berntsen, J., Aksnes, D., Ulvestad, K., 1995. Modelling the primary production in the North Sea using a coupled three-

dimensional physical-chemical-biological ocean model. Estuar. Coast. Shelf Sci. 41, 545–565.

Smith, S. V., 1997. NP budget for the Río de la Plata Estuary, Argentina/Uruguay. LOICZ-Biogeochemical Modelling Sites, LOICZ, http://data.ecology.su.se/mnode/.

Smith Jr., W. O., Demaster, D. J., 1996. Phytoplankton biomass and productivity in the Amazon river plume : correlation with seasonal river discharge. Cont. Shelf. Res. 16 (3), 291–319.

List of Figures

1 The Río de la Plata study area. The highly turbid tidal river and the outer estuary are well dissociated on this SeaWiFS image of April 28^{th} 2002. 32

2 Bathymetry of the model and morphological units of the Río de la Plata and associated shelf. Isobaths 5 m, 10 m, 20 m, 50 m and 100 m are drawn. 33

3 Tidal amplitudes (cm (a)) and co-phases (degrees (b)) of M2 from the model. Amplitudes are drawn every 10 cm, cophases every 40 degrees. 33

4 Paraná and Uruguay discharges for the January 1998 - August 2000 period, interpolated from monthly means. 34

5 Winter (a) and summer (b) mean wind stress ($N.m^{-2}$) derived from NCEP reanalysis for the period 1990-2000. Only one every three vectors is shown. 34

6 Winter (a,c,e) and summer (b,d,f) surface salinity and sections. Sections c and d are along AB transect, e and f are along AC transect. 35

7 Winter (a,c) and summer (b,d) surface chlorophyll *a* concentrations and section along the white transect. 36

8 Surface salinity (a) and chlorophyll *a* concentration (b) for the flood experiment. Isohalines 0.5, 5, 20 and 33 (lines), and isobaths (dots) 100 m, 1000 m and 2000 m are drawn. 37

9 Monthly mean situations of the Río de la Plata plume for the year 1999 (From left to right : March, June, September and December). (A) Surface salinity (0.5, 5, 10, 15, 20, 25, 30, 33 isohalines are plotted). (B) Surface chlorophyll *a* concentration ($mgChla/m^3$) from the model. (C) Surface chlorophyll *a* concentration ($mgChla/m^3$) from SeaWiFS processed by the OC5 algorithm (Gohin et al., 2002). 7, 3, 5, 6 clear images were available during March, June, September and December, respectively . (D) Integrated primary production ($gC/m^2/month$). 38

10 Surface chlorophyll *a* concentration ($mgChla/m^3$) on November 12^{th} 1999 from SeaWiFS processed with OC5 (a) and OC4 (b), and from the model (c). November integrated primary production (d). 39

11 Annual primary production in the Río de la Plata and associated shelf from the model. 400 gC/m^2/year iso-concentration is plotted and shows the highly productive area within the frontal zone of the estuary. The two white lines delimit the budgeted frontal area. 40

12 Evolution of mean monthly (a,b,c,d) and annual (e) tracer concentrations along a surface transect in the axis of the estuary. The vertical rmdotted lines delimit the frontal zone used for budget and fluxes calculations (see Fig.11). (f) Tracer concentrations at the entrance of the estuary along the year. 41

13 Limitation terms for phytoplankton growth rate in the first surface layer of the model during September (a) and December (b). Monthly mean of the maximum growth rate, the growth rate when limited by nutrients, and the growth rate when limited by light, are plotted along the transect AB of Fig.11. The vertical dotted lines delimit the frontal zone used for budget and fluxes calculations (see Fig.11). 42

14 Evolution of the different tracers concentrations in the budgeted area of Fig.11 along the year 1999. 42

15 Nitrogen fluxes (in mol $N \times 10^6$) between compartments for the area of Fig.11 during the year 1999. Values in boxes are nitrogen quantity change over the year, input from the tidal river and export to the outer estuary, at right, top and down, respectively. 43

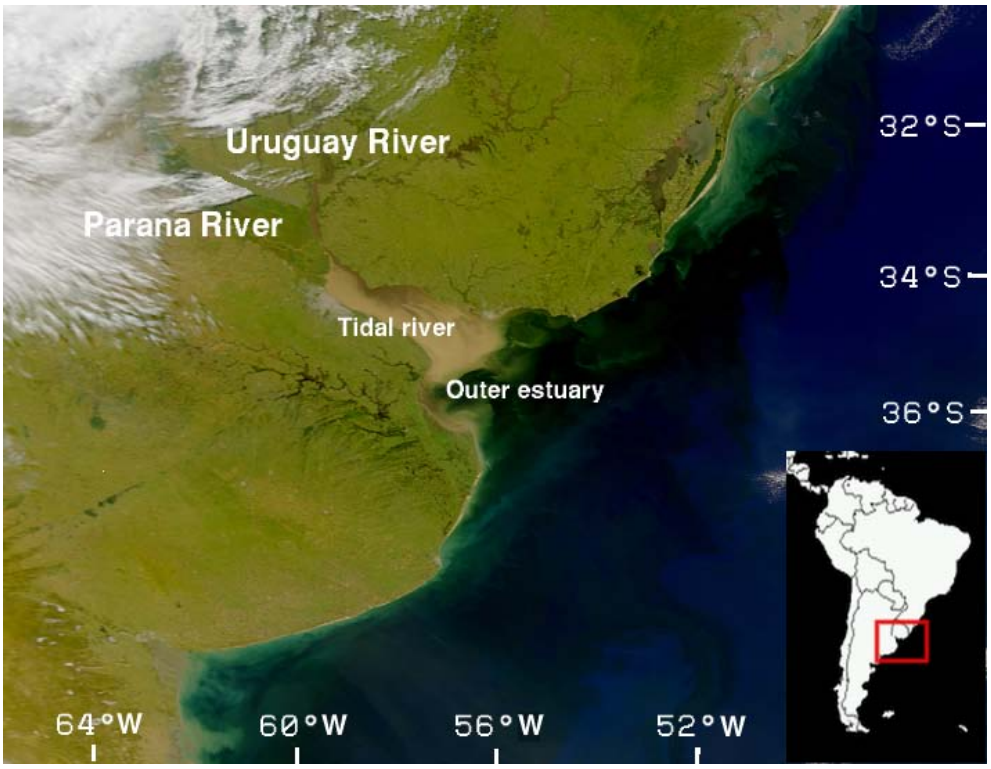

Fig. 1. The Río de la Plata study area. The highly turbid tidal river and the outer estuary are well dissociated on this SeaWiFS image of April 28^{th} 2002.

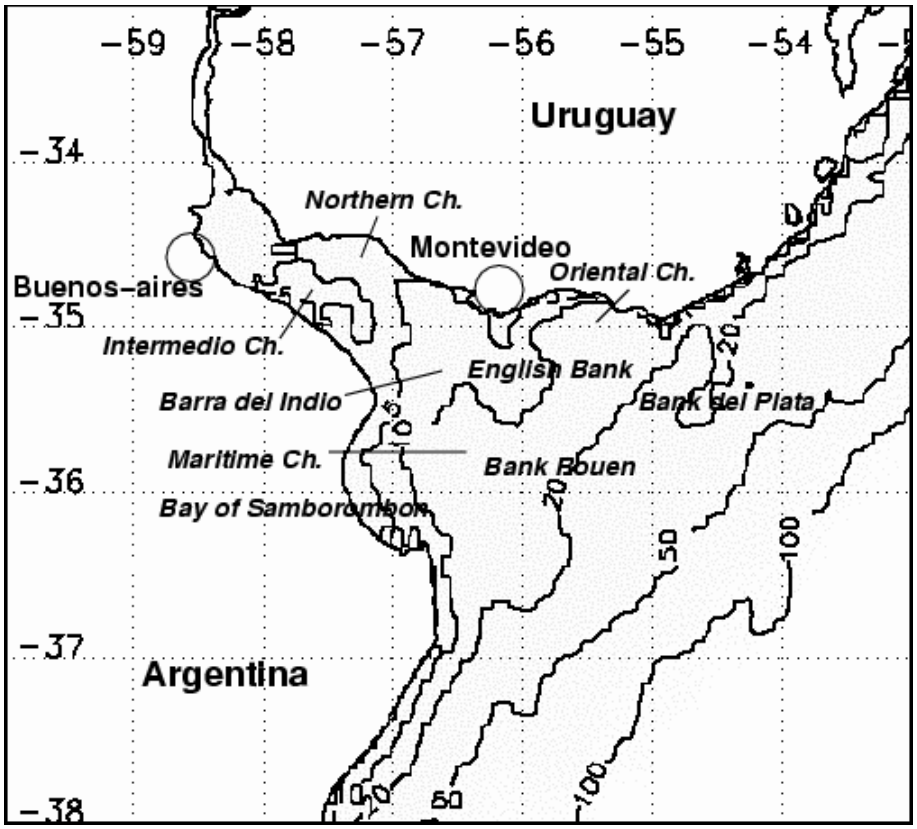

Fig. 2. Bathymetry of the model and morphological units of the Río de la Plata and associated shelf. Isobaths 5 m, 10 m, 20 m, 50 m and 100 m are drawn.

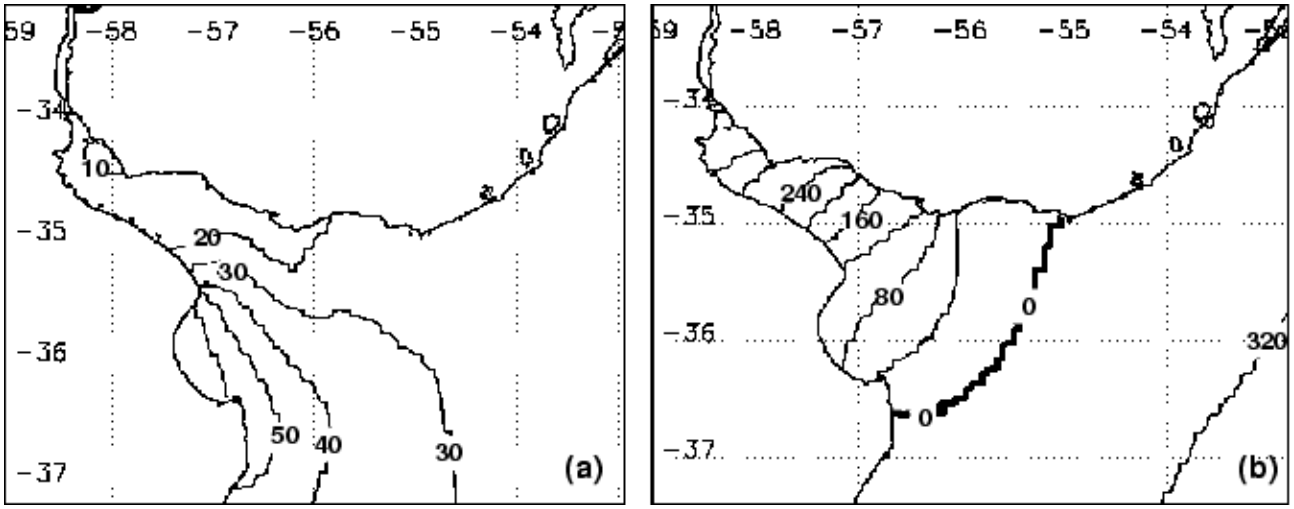

Fig. 3. Tidal amplitudes (cm (a)) and co-phases (degrees (b)) of M2 from the model. Amplitudes are drawn every 10 cm, cophases every 40 degrees.

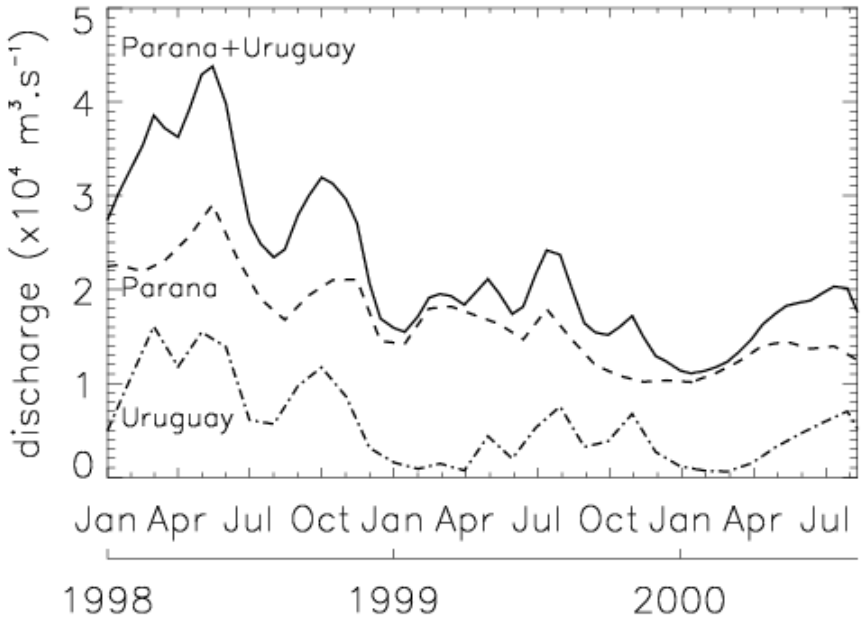

Fig. 4. Paraná and Uruguay discharges for the January 1998 - August 2000 period, interpolated from monthly means.

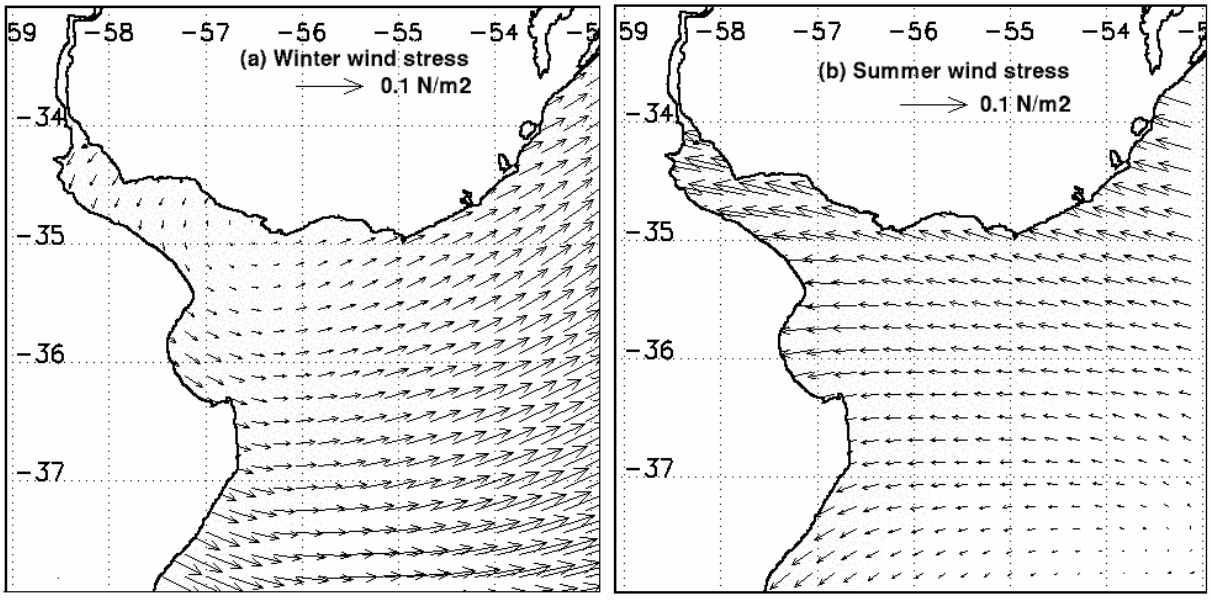

Fig. 5. Winter (a) and summer (b) mean wind stress (N.m^{-2}) derived from NCEP reanalysis for the period 1990-2000. Only one every three vectors is shown.

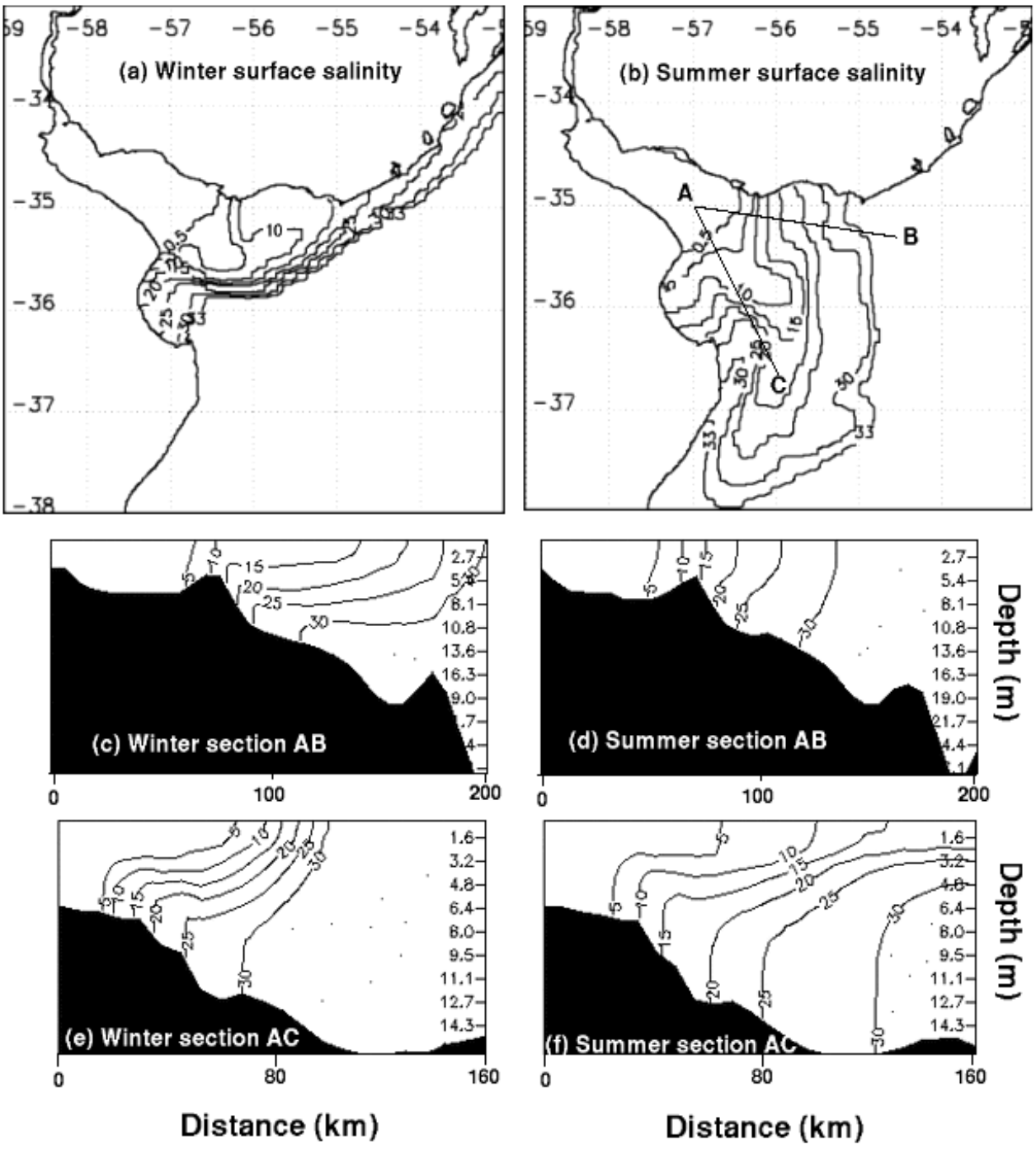

Fig. 6. Winter (a,c,e) and summer (b,d,f) surface salinity and sections. Sections c and d are along AB transect, e and f are along AC transect.

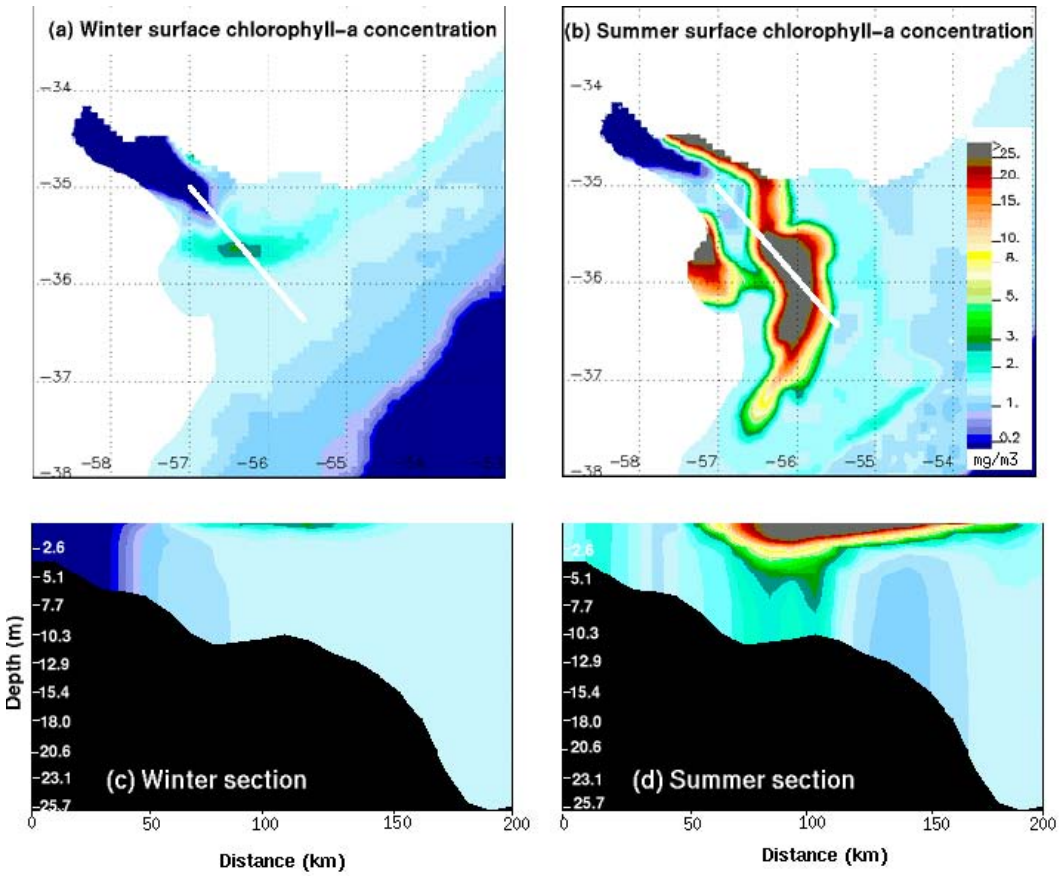

Fig. 7. Winter (a,c) and summer (b,d) surface chlorophyll *a* concentrations and section along the white transect.

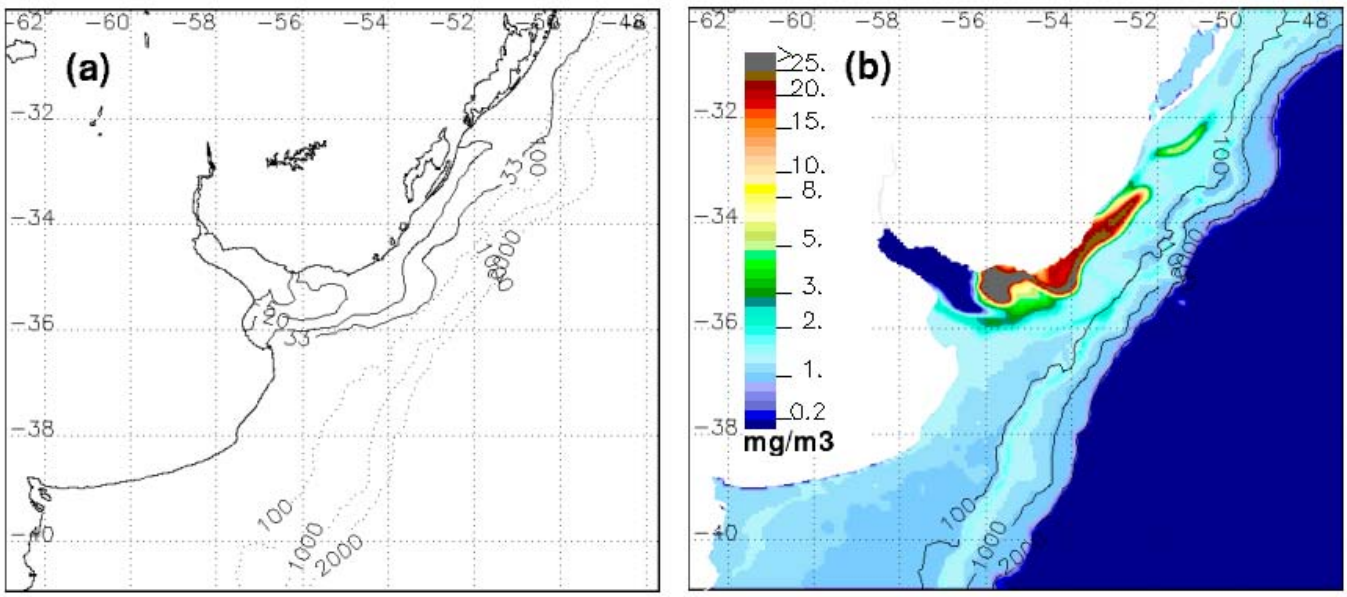

Fig. 8. Surface salinity (a) and chlorophyll *a* concentration (b) for the flood experiment. Isohalines 0.5, 5, 20 and 33 (lines), and isobaths (dots) 100 m, 1000 m and 2000 m are drawn.

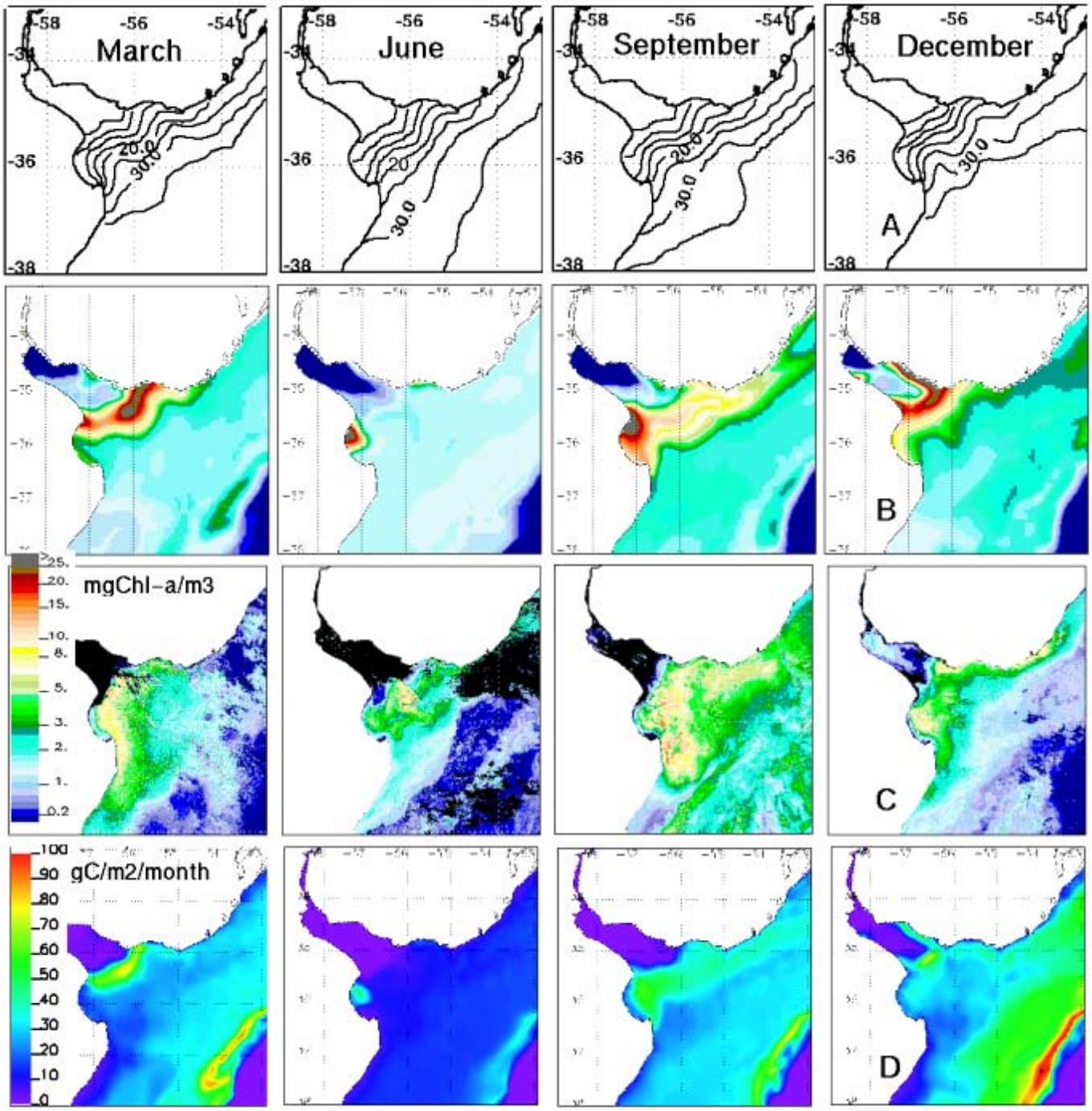

Fig. 9. Monthly mean situations of the Río de la Plata plume for the year 1999 (From left to right : March, June, September and December). (A) Surface salinity (0.5, 5, 10, 15, 20, 25, 30, 33 isohalines are plotted). (B) Surface chlorophyll *a* concentration (mgChla/m^3) from the model. (C) Surface chlorophyll *a* concentration (mgChla/m^3) from SeaWiFS processed by the OC5 algorithm (Gohin et al., 2002). 7, 3, 5, 6 clear images were available during March, June, September and December, respectively . (D) Integrated primary production (gC/m^2/month).

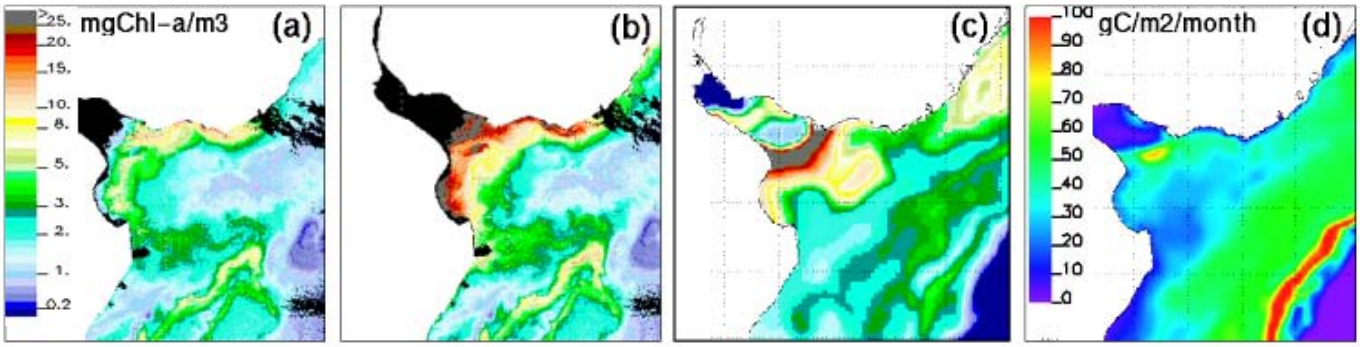

Fig. 10. Surface chlorophyll *a* concentration (mgChla/m^3) on November 12th 1999 from SeaWiFS processed with OC5 (a) and OC4 (b), and from the model (c). November integrated primary production (d).

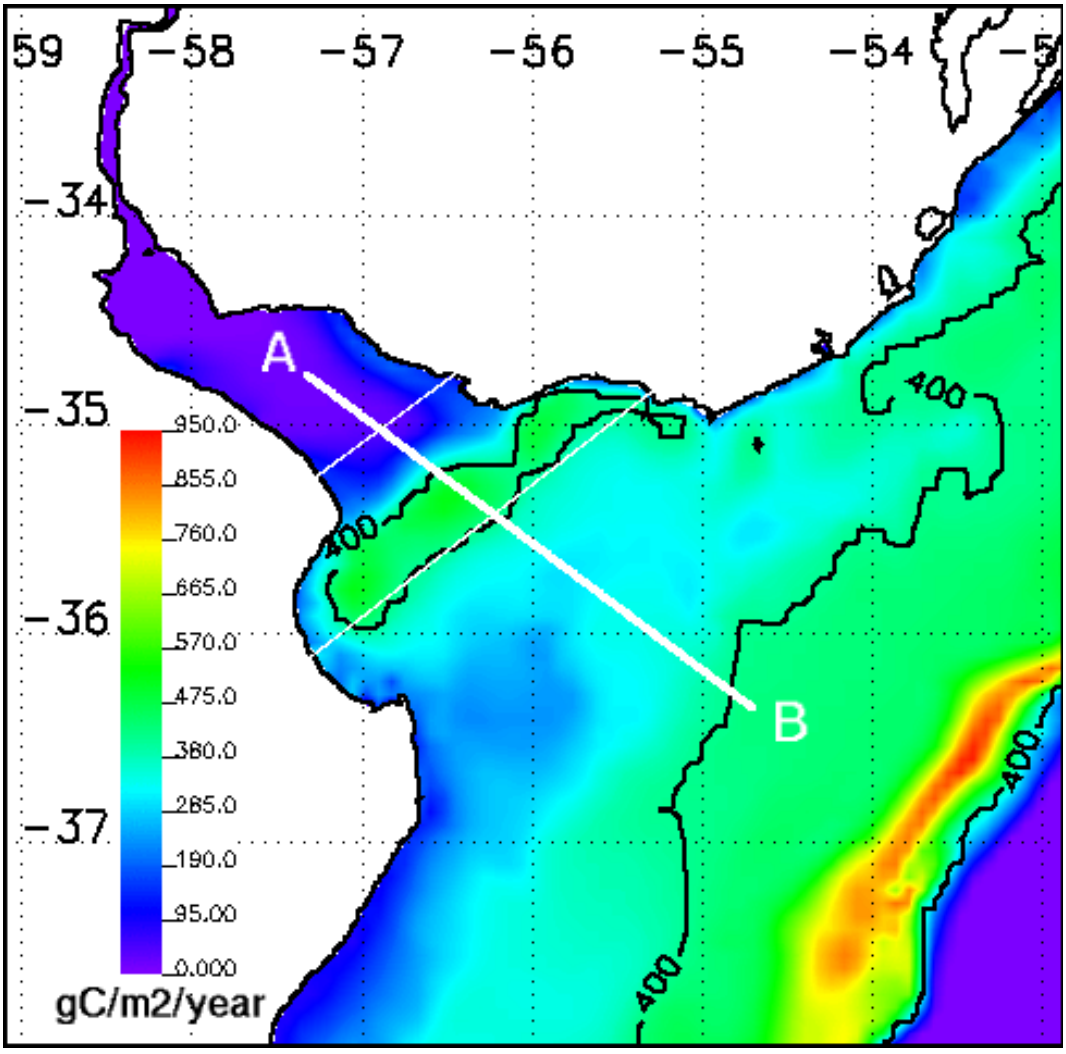

Fig. 11. Annual primary production in the Río de la Plata and associated shelf from the model. 400 gC/m^2/year iso-concentration is plotted and shows the highly productive area within the frontal zone of the estuary. The two white lines delimit the budgeted frontal area.

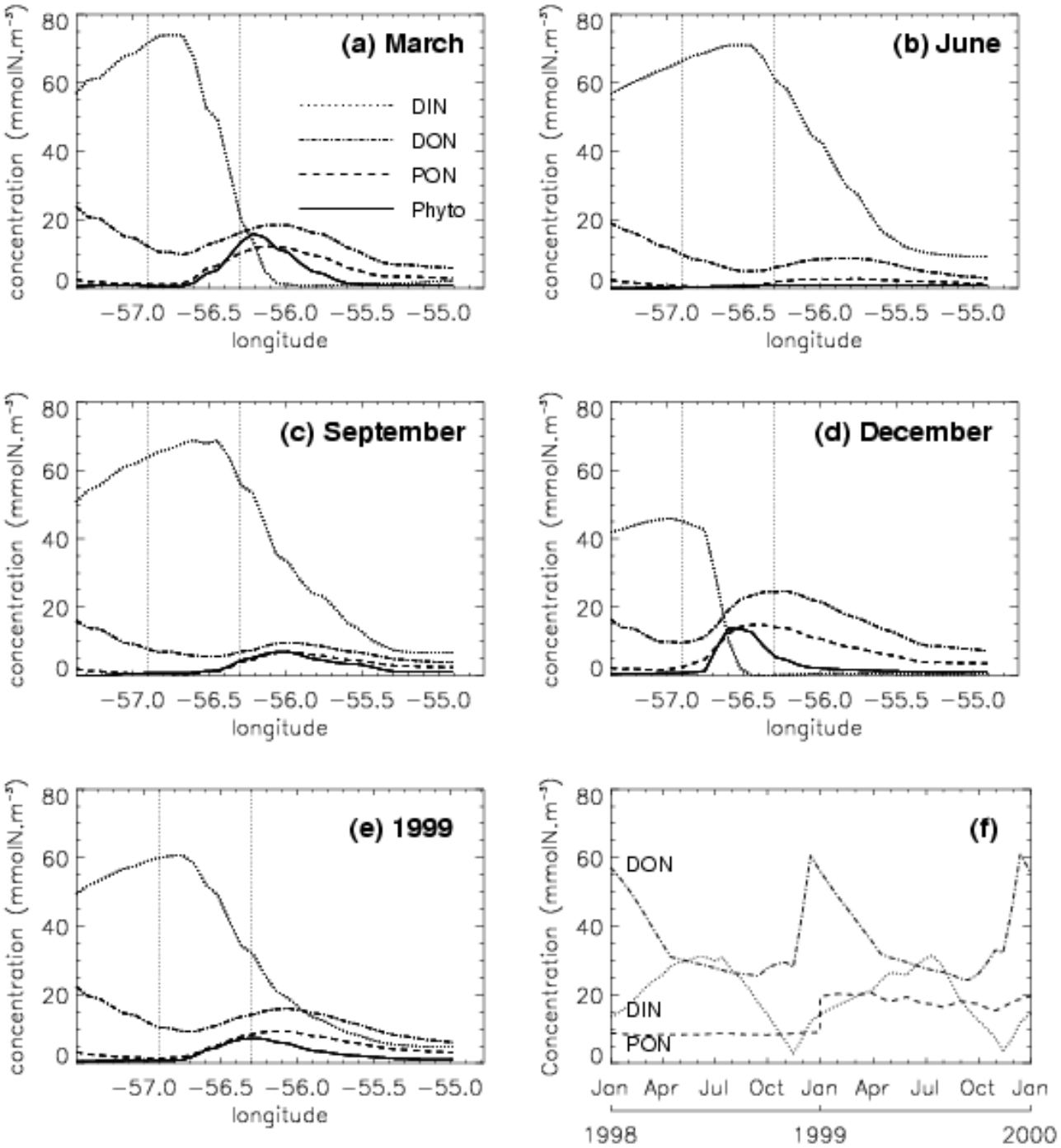

Fig. 12. Evolution of mean monthly (a,b,c,d) and annual (e) tracer concentrations along a surface transect in the axis of the estuary. The vertical rmdotted lines delimit the frontal zone used for budget and fluxes calculations (see Fig.11). (f) Tracer concentrations at the entrance of the estuary along the year.

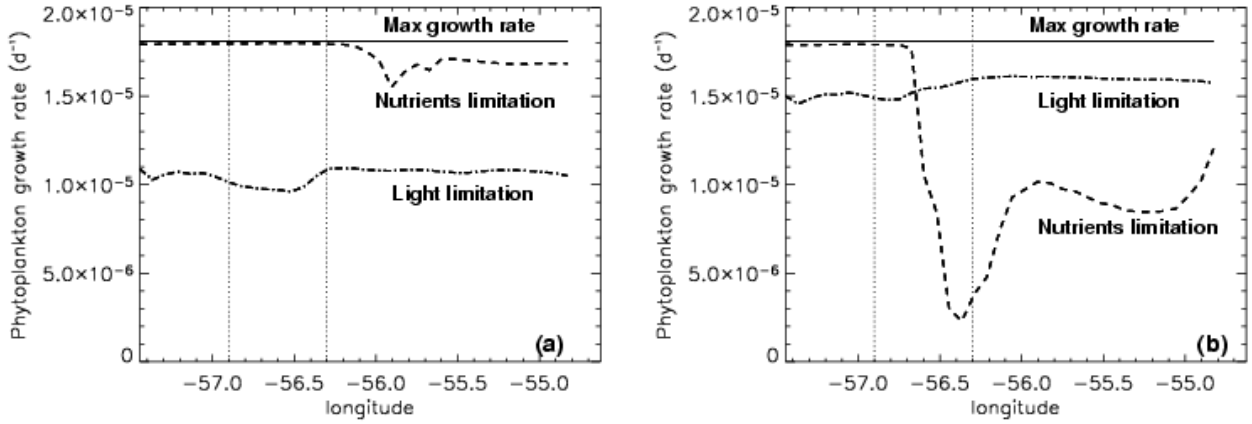

Fig. 13. Limitation terms for phytoplankton growth rate in the first surface layer of the model during September (a) and December (b). Monthly mean of the maximum growth rate, the growth rate when limited by nutrients, and the growth rate when limited by light, are plotted along the transect AB of Fig.11. The vertical dotted lines delimit the frontal zone used for budget and fluxes calculations (see Fig.11).

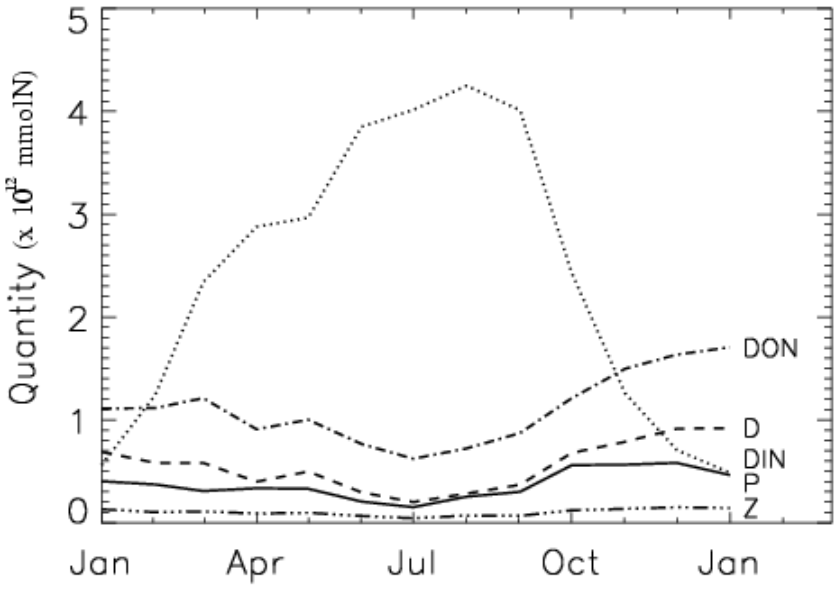

Fig. 14. Evolution of the different tracers concentrations in the budgeted area of Fig.11 along the year 1999.

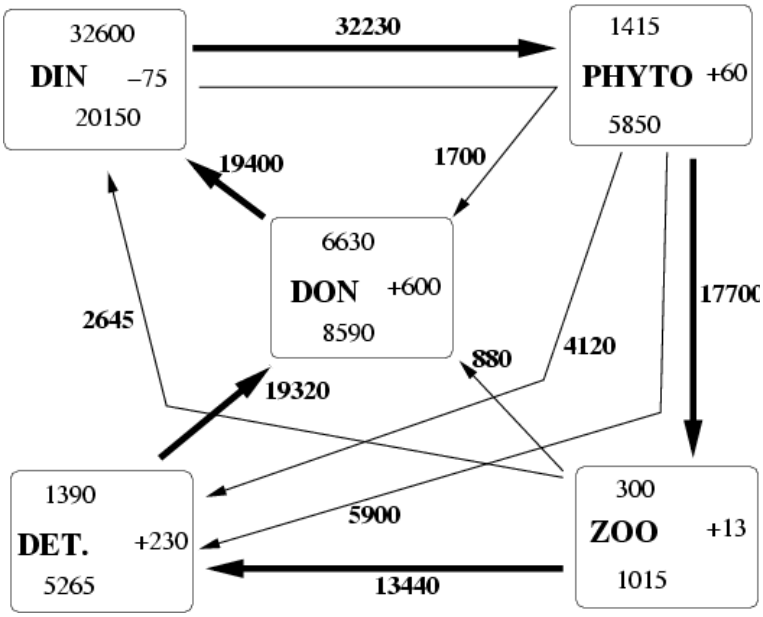

Fig. 15. Nitrogen fluxes (in mol N$\times 10^6$) between compartments for the area of Fig.11 during the year 1999. Values in boxes are nitrogen quantity change over the year, input from the tidal river and export to the outer estuary, at right, top and down, respectively.

Parameter	Symbol	Value	Unit	Reference
Phytoplankton parameters				
Initial slope of P-I curve	α	0.025	d^{-1} / Wm^{-2}	OG99
Photosynthetically active radiation coefficient	PAR	0.43		OG99
Light attenuation due to water	k_w	0.04	m^{-1}	OG99
Light attenuation by phytoplankton	k_c	0.03	m^{-1}(mmolN m^{-3})$^{-1}$	OG99
Light attenuation by suspended particulate matter	k_{spm}	0.005	m^{-1} (gm^{-3})$^{-1}$	adjusted
Exudation fraction of primary production	ε	0.05		F90
Maximum growth rate parameters	a	0.6	d^{-1}	OG99
	b	1.066		OG99
	c	1.0	$(C)^{-1}$	OG99
Half saturation constant for N uptake	k_N	0.5	mmolN m^{-3}	OG99
Specific mortality rate	μ_p	0.03	d^{-1}	OG99
Zooplankton parameters				
Assimilation efficiency	f_1	0.75		OG99
Maximum grazing rate	g	0.75	d^{-1}	adjusted
Prey capture rate	p	1.0	(mmolN m^{-3})$^{-2}$ d^{-1}	OG99
Mortality	μ_z	0.2	(mmolN m^{-3})$^{-2}$ d^{-1}	OG99
Excretion rate	γ	0.1	d^{-1}	adjusted
Organic fraction of excretion	f_2	0.25		F90
Detritus parameters				
Hydrolysis rate	μ_d	0.1	d^{-1}	adjusted
Sinking velocity	w_s	5	m d^{-1}	OG99
DON parameters				
remineralization rate	ρ	0.05	d^{-1}	adjusted

Table 1
Parameters of the ecosystem model. (OG99 : (Oschlies and Garçon, 1999), F90 : (Fasham et al., 1990))

Configuration	Winter (July-Aug)	Summer (Jan-Feb)	Flood experiment
Wind (NCEP climatology 1990-2000)	July-August	January-February	no wind
Net shortwave radiation (W/m^2)	120	250	120
	(July-August)	(January-February)	
Discharge (mean 1990-2000) (m^3/s)	22 496	20 714	40 000
Paraná contribution	16 811	16 836	
Uruguay contribution	5 685	3 878	
River nutrients supply (mg/l)			
DIN		0.25	
DON		0.6	
PON		0.25	
Surface initial conditions			
DIN (mmol N/m^3)		5 (up to 30 at 5000 m)	
DON (mmol N/m^3)		10^{-4}	
PON (mmol N/m^3)		10^{-4}	
Zooplankton (mmol N/m^3)		6.10^{-3}	
Chlorophyll *a* (mg/m^3)		0.5	

Table 2
Configurations for the climatological simulations.